FIG. 6. Patient 5. Clinical photographs of the left hand at age 1 month (A); the hands at age 19 years (B); the right (C) and the left (D) feet at age 1 month; the feet at age 19 years (E); the skin on the back of the left hand at age 19 years (F); the left elbow at age 19 years (G); and a massive subcutaneous hematoma at age 16 years (H). Radiographs of the left (I,J) and the right (K,L) hands, and the spine (M,N) at age 19 years. Arrows indicate ectipic calcification (K,N). [Color figure can be viewed in the online issue, which is available at www.interscience.wiley.com.]

from infectious endocarditis, treated with surgical resection of vegetations and long-term administration of antibiotics. Menstruation, beginning at age 14 years, was irregular. She developed a massive subcutaneous hematoma in the right calf at age 16 years (Fig. 6H), and over the skull after a mild injury at age 17 years, necessitating admission in an ICU and transfusion of packed red cells. She frequently had subcutaneous infections with fistula formation at the elbows and the buttocks, treated with intravenous administration of antibiotics.

When seen by us at age 19 years, her weight was 47 kg (−0.8 SD) and height 158.5 cm (−0.1 SD). She had a slightly asymmetric and slender face with hypertelorism, blue sclerae, strabismus, a short nose with a hypoplastic columella, low-set ears, a small mouth, a high and narrow palate, crowded teeth, and a mildly protruding jaw. She had pectus excavatum, cylindrical fingers with hyper-extensibility and flexion-adduction contractures of bilateral thumbs (Fig. 6B), chronic dislocations of bilateral distal radio-ulnar joints and radial heads, and talipes valgus and planus with

extremely soft subcutaneous tissues at the heels (Fig. 6E), causing difficulty in walking. Her skin was hyperextensible (Fig. 6F), bruisable, and fragile with atrophic scars (Fig. 6G); and showed hyperalgesia to pressure. Fine palmar creases were also noted. Cardiac ultrasonography showed both aortic and mitral valve regurgitation. Abdominal ultrasonography showed nephrolithiasis. Ophthalmological examinations showed myopia and astigmatism, as well as a mild elevation of IOP accompanied by mild visual field loss.

Patient 6

The patient, now a 4-year-old Japanese girl, was the first child of a healthy mother and a healthy non-consanguineous father, both 29 years of age. She was born by vaginal delivery with minimal labor induction at 41 weeks and 5 days of gestation. Her birth weight was 3,004 g (-0.5 SD), length 48.0 cm (-1.2 SD), and OFC 33.0 cm (-0.6 SD). She was admitted in a neonatal ICU for the evaluation and treatment of orthopedic complications, including flexion-adduction contractures of bilateral thumbs, extension contractures of bilateral index to little fingers, flexion contractures of bilateral wrists, rigidity of bilateral hip joints, and bilateral talipes equinovarus. A large anterior fontanelle and diastasis recti with an umbilical hernia were also noted. She showed no spontaneous defecation and required a laxative suppository every day. Her initial clinical diagnosis was Freeman–Sheldon syndrome. Bilateral talipes equinovarus and finger-wrist contractures were treated with serial plaster casts, followed by a surgical correction of the left talipes equinovarus at age 1 year. Atrophy of the flexor hallucis longus muscle was noted. Skin fragility was noticed at the operation, and she was suspected to have EDS. She raised her head at age 5 months, sat unassisted and rolled over at age 9 months, and walked independently at age 1 year and 5 months. Developmental quotient at age 10 months was 64 in physical/motor, 100 in manipulation, 82 in receptive language, 55 in expressive language, 100 in social relationships with adults, and 100 in feeding. Brain and spine MRI, for evaluating delayed closure of the anterior fontanelle, showed tethering of a spinal cord at L3-4 level (normal, L1-2) at age 1 year and 6 months. She underwent duraplasty and resection of protruded coccyges at age 1 year and 11 months. Around age 3 years, she did not need to have laxative suppositories for constipation but only oral magnesium oxide. At age 3 years and 1 month, a subcutaneous cyst appeared at the sacral region, which was resected surgically. At age 3 years and 11 months, a sacral abscess occurred and was treated with surgical drainage, followed by recurrent subcutaneous infections and fistula formation. Two calcified nodules were detected in the abscess. Ophthalmological examinations showed bilateral decreased visual acuity, myopia, astigmatism, and elevated IOP (26 mmHg in the right eye; 29 mmHg in the left), treated with topical administration of a beta-adrenergic receptor blocker (carteolol). Otological examinations showed mild hearing impairment of high-pitched sound with a threshold of 30 dB at 1 kHz and 40 dB at 4 kHz.

When seen by us at age 4 years, her weight was 13.0 kg (-1.3 SD), height 96.2 cm (-1.2 SD), and OFC 49.0 cm (-0.9 SD). Her facial characteristics included hypertelorism, blue sclerae, strabismus, short palpebral fissures, a short and depressed nose with a hypoplastic columella, low-set and rotated ears, redundant cheeks, a long philtrum, a thin upper lip vermilion, and a high palate. Her skin was hyperextensible (Fig. 7D) and bruisable, but only one traumatic would was noticed with an atrophic scar. She had fine palmer creases of hands and could not flex or extend the DIP joints in all fingers (Fig. 7A,B). She had talipes planus, slender and immobile toes, and soft subcutaneous tissues at the heels (Fig. 7C). A mild pectus excavatum and widely spaced nipples were also observed. She hated to be hugged tightly, suggesting hyperalgesia to pressure.

RADIOLOGICAL EXAMINATIONS

Radiographs of hands were available in Patient 1 at age 16 years (Fig. 1O), Patient 2 at age 28 years (Fig. 2L,M), Patient 3 at age 31 years (Fig. 4L,M), and Patient 5 at age 19 years (Fig. 6I–L). Diaphyseal narrowing of the phalanges and metacarpals, and dislocations of bilateral distal radio-ulnar joints were noted. Radiographs of feet were available in Patient 1 at age 16 years (Fig. 1P), Patient 2 at age 28 years (Fig. 2N), and Patient 6 at age 4 years (Fig. 7E–H). Talipes valgus and planus or cavum, with diaphysial narrowing of the phalanges and metatarsals, were noted. Radiographs of spines were available in all patients. Variable degrees of scoliosis or kyphoscoliosis and decreased physiological kyphosis of thoracic spines with tall vertebral bodies were noted: Patient 1 at age 16 years (Fig. 1Q,R; scoliosis with a Cobb angle of 32° at T12-L4, kyphosis with a kyphotic angle of 72° at T11-L3), Patient 2 at age 28 years (Fig. 2O,P; scoliosis with a Cobb angle of 27° at C7-T8, 20° at T8-T12, 15° at T12-L4), Patient 3 at age 31 years (Fig. 4N; scoliosis with a Cobb angle of 8° at T4-T12 and 6° at T12-L4), Patient 4 at age 31 years (Fig. 5; scoliosis with a Cobb angle, of 10° at T1-T10), Patient 5 at age 19 years (Fig. 6M,N; scoliosis with a Cobb angle of 12° at T3-T11), and Patient 6 at age 2 years (Fig. 7I,J; scoliosis with a Cobb angle of 6° at T5-L2). Ectopic calcification was noted in Patients 2 and 5 (Figs. 2M and 6K,N).

BIOCHEMICAL SCREENING

Biosynthesis of procollagens I and III on cultured dermal fibroblasts from Patients 1, 3, 5, and 6 was analyzed as described previously [Hata et al., 1988]. Fibroblasts of all four patients showed normal production of type I and type III procollagens (data not shown), excluding vascular type EDS.

Urinary pyridinoline and deoxypyridinoline excretion was evaluated with HPLC in Patients 1 and 5 as described previously [Pasquali, 1994; Steinmann, 1995]. Normal deoxypyridinoline to pyridinoline ratio was observed in both patients (data not shown), excluding kyphoscoliosis type EDS.

GENETIC SCREENING

G-banded chromosomes were normal in Patients 1, 2, and 6. Direct sequencing of *TGFBR1* and *TGFBR2*, according to the method by Sakai et al. [2006], showed no mutation in Patients 1 and 2.
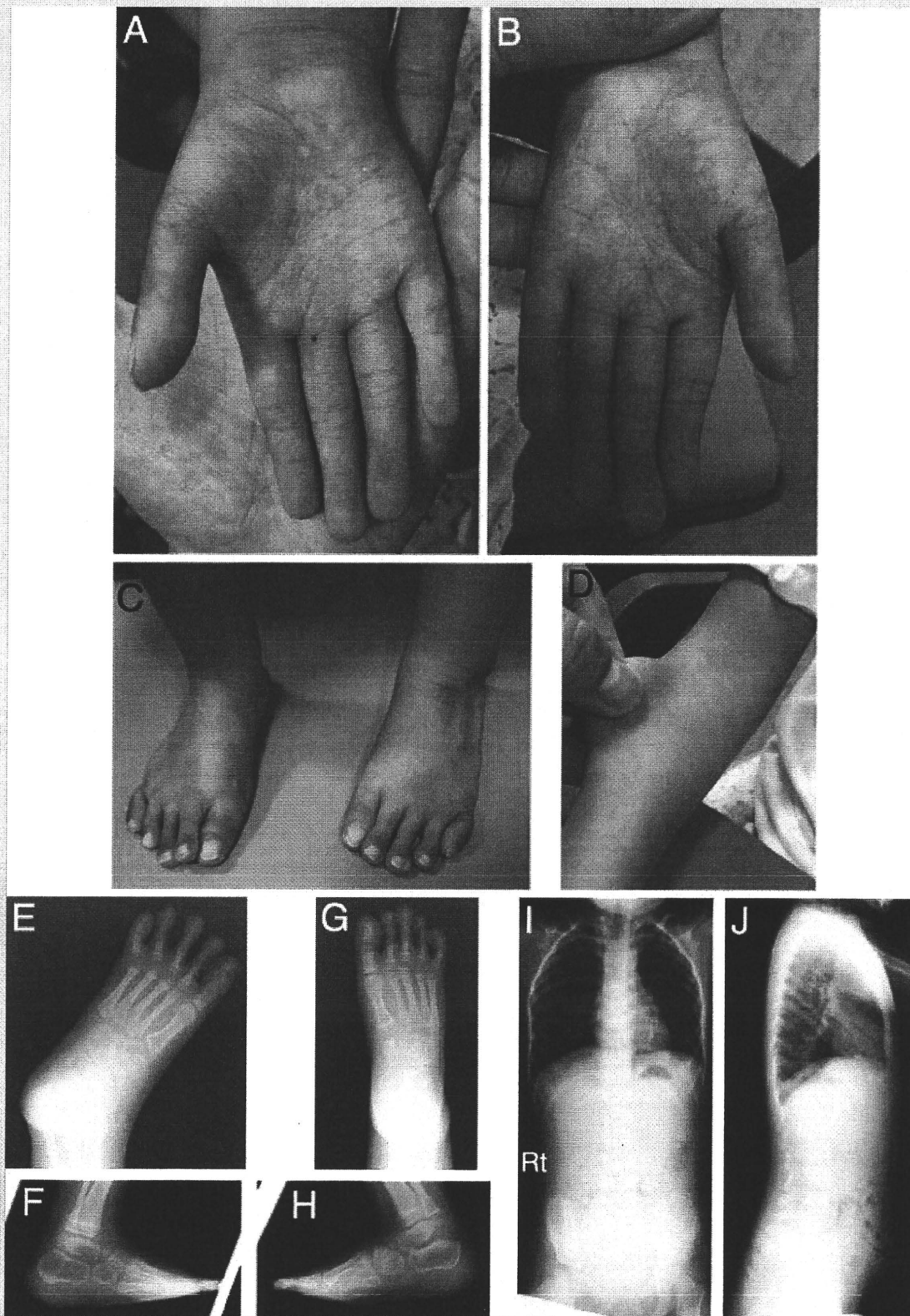
FIG. 7. Patient 6. Clinical photographs, at age 4 years, of the right (A) and the left (B) hands; the feet (C); and the skin on the right forearm (D). Radiographs of the left (E,F) and the right (G,H) feet at age 4 years and the spine at age 2 years (I,J). [Color figure can be viewed in the online issue, which is available at www.interscience.wiley.com.]

DISCUSSION

Clinical features of the six patients are summarized in Table I. Strikingly similar manifestations occur according to the ages, including: (1) *Craniofacial*: large fontanelle, hypertelorism, short and downslanting palpebral fissures, blue sclerae, short nose with hypoplastic columella, low-set and rotated ears, high palate, long philtrum, thin upper lip vermilion, small mouth, and micro-retrognathia in infancy; slender and asymmetric face with protruding jaw from adolescence; (2) *Skeletal*: congenital

TABLE I. Clinical Features of the Six Patients

	Patient 1	Patient 2	Patient 3	Patient 4	Patient 5	Patient 6
Age (years)/sex	16/F	32/F	32/M	32/M	20/F	4/F
Consanguinity	−	+	+	NI	−	−
Craniofacial						
Large fontanelle in infancy	+	+	+	NI	+	+
Hypertelorism	+	+	+	+	+	+
Blue sclerae	+	+	+	+	+	+
Short nose with hypoplastic columella	+	+	+	NI	+	+
Low-set ears	+	+	+	NI	+	+
High-arched palate	+	+	+	+	+	+
Long philtrum and thin upper lip	+	+	+	NI	+	+
Small mouth/micro-retrognathia in infancy	+	+	+	NI	+	NI
Slender face/protruding jaw from adolescence	+	+	+	+	+	NI
Facial asymmetricity from adolescence	+	+	+	+	+	NI
Skeletal						
Congenital multiple contractures	+	+	+	NI	+	+
Tendon abnormalities	+	+	+	NI	+	NI
Recurrent joint dislocations	+	+	+	−	+	−
Pectus deformities	Excavatum	Flat, thin	Flat, thin	Excavatum	Excavatum	Excavatum
Spinal deformities	Kyphoscoliosis	Scoliosis	Kyphoscoliosis	Kyphoscoliosis	Scoliosis	Scoliosis
Slender and/or cylindrical fingers	+	+	+	+	+	+
Progressive talipes deformities	Planus, valgus	Cavus, valgus	Planus, valgus	Planus, valgus	Planus, valgus	Planus
Skin						
Hyperextensibility	+	+	+	+	+	+
Bruisability	+	+	+	+	+	+
Fragility (atrophic scars)	+	+	+	−	+	+
Hyperalgesia to pressure	+	+	+	−	+	+
Fine/acrogeria-like palmar creases	+	+	+	+	+	+
Recurrent subcutaneous infections/fistula formation	+	+	+	−	+	+
Cardiovascular						
Valve abnormalities	ASD, TR, TVP, MVP	−	AR, MR	−	AR, MR, IE	NI
Large subcutaneous hematomas	+	+	+	+	+	−
Respiratory						
(Hemo) pneumothorax	−	+	+	+	−	−
Gastrointestinal						
Constipation	+	+	+	−	+	+
Diverticular perforation	−	+	+	−	−	−
Ophthalmological						
Strabismus	+	+	+	−	+	+
Glaucoma	−	+	−	−	+	+
Refractive errors	Hyperopia	Myopia Astigmatism	Myopia Astigmatism	−	Myopia Astigmatism	Myopia Astigmatism
Hearing impairment	+	+	+	−	−	+
Motor function						
Gross motor developmental delay	+	+	+	NI	+	+

Patients 1 and 2 were reported by Kosho et al. [2005] and Patient 4 was reported by Yasui et al. [2003].
F, female; M, male; −, absent; +: present; NI, no information available; ASD, atrial septal defect; TR, tricuspid valve regurgitation; TVP, tricuspid valve prolapse; MVP, mitral valve prolapse; AR, aortic valve regurgitation; MR, mitral valve regurgitation; IE, infectious endocarditis.

contractures of fingers, wrists, hips, and feet (talipes equinovarus) with anomalous insertions of flexor muscles; progressive joint laxity with recurrent dislocations; slender and/or cylindrical fingers and progressive talipes valgus and cavum or planus, with diaphyseal narrowing of the phalanges, metacarpals, and metatarsals; inability to move fingers and toes separately or smoothly; pectus deformities (flat or excavated); scoliosis or kyphoscoliosis with decreased physiological curvatures of thoracic spines and tall vertebrae; (3) *Cutaneous*: progressive hyperextensibility, bruisability, and fragility with atrophic scars; fine palmar creases from childhood to adolescence and prominent palmar wrinkles showing acrogeria in adulthood; recurrent subcutaneous infections with fistula formation; (4) *Cardiovascular*: cardiac valve abnormalities; recurrent large subcutaneous hematomas from childhood; (5) *Gastrointestinal*: constipation, diverticula perforation; (6) *Respiratory*: (hemo) pneumothorax; (7) *Ophthalmological*: strabismus, glaucoma, refractive errors. Hearing impairment of high-pitched sounds and gross developmental delay are also frequent. Initial diagnosis was Freeman–Sheldon syndrome in Patients 2 and 6, arthrogryposis in Patient 3, and EDS in the others, according to predominant manifestations with ages. In view of these findings, it is reasonable to consider that the patients would share a single disorder consisting of four clinical elements: craniofacial characteristics, congenital multiple contractures, progressive joint and skin laxity, and progressive multisystem tissue fragility. Parental consanguinity in two patients suggested an autosomal recessive mode of inheritance.

The disorder shows all hallmarks of EDS, which are skin hyperextensibility, joint hypermobility, and tissue fragility affecting skin, ligaments, joints, blood vessels, and internal organs [Steinmann et al., 2002]. Characteristic faces are noted in vascular type (thin, delicate, and pinched nose; thin lips; tight skin; hollow cheeks; prominent staring eyes; and tight, firm, lobeless ears) [Beighton et al., 1998; Steinmann et al., 2002], dermatosparaxis type (puffy eyelids with excessive periorbital skin, and large fontanelle) [Steinmann et al., 2002], progenoid form (frontal bossing, sparse scalp hair, prominent eyes, down-slanting palpebral fissures, midface hypoplasia, and small mouth) [Faiyaz-Ul-Haque et al., 2004], and EDS-like spondylocheirodysplasia (down-slanting palpebral fissures, protruding eyes, and blue sclerae) [Giunta et al., 2008], all of which could be distinguishable from our series. Congenital contractures are noted in vascular type (talipes equinovarus), kyphoscoliosis type (talipes equinovarus), arthrochalasia type (hip dislocation) [Beighton et al., 1998; Steinmann et al., 2002], and EDS-like spondylocheirodysplasia (finger contractures and talipes equinovarus) [Giunta et al., 2008]; but distinct finger-wrist contractures or progressive talipes valgus and cavum or planus after corrections of equinovarus, observed in our series, have not been described. Spinal deformities are noted in kyphoscoliosis type (kyphoscoliosis), arthrochalasia type (kyphoscoliosis) [Beighton et al., 1998; Steinmann et al., 2002], and EDS-like spondylocheirodysplasia (platyspondyly, osteopenia, and irregular endplates) [Giunta et al., 2008], whereas decreased physiological curvatures of thoracic spines and tall vertebrae have not been described. Skin hyperextensibility, bruisability, and fragility with atrophic scars in our series were similar to classical type, kyphoscoliosis type, and arthrochalasia type [Beighton et al., 1998; Steinmann et al., 2002], but prominent palmar wrinkles in our adult patients have not been

described in previous EDS types. Recurrent large subcutaneous hematomas, occurring after childhood, were the most serious complications in our series, which could have been fatal if the treatment (transfusion of packed red cells or emergency surgical drainage) had been delayed. Superficial or intramuscular small arteries were supposed to be ruptured after minor injuries, followed by acute spread of hemorrhage because of markedly loose subcutaneous tissue. Arterial lesions (dissection, aneurysm, and rupture) are the most important complications in vascular type and occasional but the major life-threatening complications in kyphoscoliosis type. However, aorta, branches of aorta, and major arteries in limbs have been affected in vascular type [Oderich et al., 2005]; and aorta and medium-sized arteries (middle cerebral artery, vertebral artery, femoral artery, and intrathoracic artery) have been affected in kyphoscoliosis type [Wenstrup et al., 1989; Steinmann et al., 2002; Yeowell and Steinmann, 2008]. Normal production of type I and III procollagen excluded vascular type and normal urinary deoxypyridinoline to pyridinoline ratio evaluated with HPLC excluded kyphoscoliosis type. Furthermore, this condition is distinguishable to other connective tissue disorders such as Marfan syndrome (MFS) [Dietz, 2009] and Loeys–Dietz syndrome (LDS) [Loeys and Dietz, 2008]. Although *FBN1* molecular analysis was not performed in our series, distinct facial characteristics and profound skin and joint laxity as well as other serious multisystem complications have never been reported in MFS. No mutation in *TGFBR1* or *TGFBR2* excluded LDS.

Present patients shared many clinical features with a Pakistani sister and brother reported by Steinmann et al., [1975], including characteristic face (a slender and asymmetric face with hypertelorism, downslanting palpebral fissures, blue sclerae, a short nose with a hypoplastic columella, a high palate, a long philtrum, and a small mouth in the brother at age 18 years); talipes equinovarus and progressive talipes vagus and planus after corrections; joint laxity; scoliosis or kyphoscoliosis with tall vertebral bodies; arachnodactyly with diaphysial narrowing of phalanges, metacarpals, and metatarsals; skin hyperextensibility, bruisability, and fragility with atrophic scars; hyperalgesia to pressure; and delayed motor development. The sibs have been classified into a subtype of kyphoscoliosis type EDS [Steinmann et al., 2002], though lysyl hydroxylase activity was proved to be normal [Wenstrup et al., 1989].

In conclusion, we propose that these present patients represent a new clinically recognizable type of EDS characterized by distinct craniofacial features, multiple congenital contractures, progressive joint and skin laxity, and progressive multisystem fragility-related manifestations, including recurrent large subcutaneous hematomas and other cardiac, respiratory, gastrointestinal, ophthalmological complications.

ACKNOWLEDGMENTS

REFERENCES

Abu A, Frydman M, Marek D, Pras E, Nir U, Reznik-Wolf H, Pras E. 2008. Deleterious mutations in the zinc-finger 469 gene cause brittle cornea syndrome. Am J Hum Genet 82:1217–1222.

Beighton P, De Paepe A, Steinmann B, Tsipouras P, Wenstrup R. 1998. Ehlers-Danlos syndromes: Revised nosology, Villefranche, 1997. Am J Med Genet 77:31–37.

Dietz HC. 2009. Marfan syndrome. In: GeneReviews at genetests: Medical Genetics Information Resource (database online).Copyright, University of Washington. Seattle: 1997–2009. Available at http://www.genetests. org. Accessed April 11, 2010.

Faiyaz-Ul-Haque M, Zaidi SHE, Al-Ali M, Al-Mureikhi MS, Kennedy S, Al-Thani G, Tsui LC, Teebi AS. 2004. A novel missense mutation in the galactosyltransferase-I (*B4GALT7*) gene in a family exhibiting facioskeletal anomalies and Ehlers-Danlos syndrome resembling the progeroid type. Am J Med Genet Part A 128A:39–45.

Giunta C, Elioglu NH, Albrecht B, Eich G, Chambaz C, Janecke A, Yeowell H, Weis MA, Eyre DR, Kraenzlin M, Steinmann B. 2008. Spondylocheiro dysplastic form of the Ehlers-Danlos syndrome-an autosomal recessive entity caused by mutations in the zinc transporter gene SLC39A13. Am J Hum Genet 82:1290–1305.

Hata R, Kurata S, Shinkai H. 1988. Existence of malfunctioning pro alpha 2(I) collagen genes in a patient with pro alpha 2(I)-chain-defective variant of Ehlers-Danlos syndrome. Eur J Biochem 174:231–237.

Kosho T, Takahashi J, Ohashi H, Nishimura G, Kato H, Fukushima Y. 2005. Ehlers-Danlos syndrome type VIB with characteristic facies, decreased curvatures of the spinal column, and joint contractures in two unrelated girls. Am J Med Genet Part A 138A:282–287.

Kresse H, Rosthoj S, Quentin E, Hollmann J, Glossl J, Okada S, Tonnesen T. 1987. Am J Hum Genet 41:436–453.

Loeys BL, Dietz HC, 2008. Loeys-Dietz syndrome. In: GeneReviews at genetests: Medical Genetics Information Resource (database online). Copyright, University of Washington, Seattle 1997–2009. Available at http: //www.genetests.org. Accessed April 11, 2010.

Mao JR, Bristow J. 2001. The Ehlers-Danlos syndrome: On beyond collagens. J Clin Invest 107:1063–1069.

Oderich GS, Panneton JM, Bower TC, Lindor NM, Cherry KJ, Noel AA, Kalra M, Sullivan T, Gloviczki P. 2005. The spectrum, management and clinical outcome of Ehlers-Danlos syndrome type IV: A 30-year experience. J Vasc Surg 42:98–106.

Pasquali M. 1994. Urinary pyridinium cross-links: A non invasive diagnostic test for Ehlers-Danlos syndrome type VI. N Engl J Med 331: 132–133.

Sakai H, Visser R, Ikegawa S, Ito E, Numabe H, Watanabe Y, Mikami H, Kondoh T, Kitoh H, Sugiyama R, Okamoto N, Ogata T, Fodde R, Mizuno S, Takamura K, Egashira M, Sasaki N, Watanabe S, Nishimaki S, Takada F, Nagai T, Okada Y, Aoka Y, Yasuda K, Iwasa M, Kogaki S, Harada N, Mizuguchi T, Matsumoto N. 2006. Comprehensive genetic analysis of relevant four genes in 49 patients with Marfan syndrome or Marfan-related phenotypes. Am J Med Genet Part A 140A:1719–1725.

Schalkwijk J, Zweers MC, Steijlen PM, Dean WB, Taylor G, van Vlijmen IM, van Haren B, Miller WL, Bristow J. 2001. A recessive form of the Ehlers-Danlos syndrome caused by tenascin-X deficiency. N Engl J Med 345:1167–1175.

Schwarze U, Hata R, McKusick VA, Shinkai H, Hoyme HE, Pyeritz RE, Byers PH. 2004. Rare autosomal recessive cardiac valvular form of Ehlers-Danlos syndrome results from mutations in the COL1A2 gene that activate the nonsense-mediated RNA decay pathway. Am J Hum Genet 74:917–930.

Steinmann B. 1995. Urinary pyridinoline cross-links in Ehlers-Danlos syndrome type VI. Am J Hum Genet 57:1505–1508.

Steinmann B, Gitzelmann R, Vogel A, Grant ME, Harwood R, Sear CHJ. 1975. Ehlers-Danlos syndrome in two siblings with deficient lysyl hydroxylase activity in cultured skin fibroblasts but only mild hydroxylysine deficit in skin. Helv Paediat Acta 30:255–274.

Steinmann B, Royce PM, Superti-Furga A. 2002. The Ehlers-Danlos syndrome. In: Royce PM, Steinmann B, editors. Connective tissue and its heritable disorders. New York: Wiley-Liss. pp. 431–523.

Wenstrup RJ, Murad S, Pinnell SR. 1989. Ehlers-Danlos syndrome typw IV: Clinical manifestations of collagen lysyl hydroxylase deficiency. J Pediatr 115:405–409.

Yasui H, Adachi Y, Minami T, Ishida T, Kato Y, Imai K. 2003. Combination therapy of DDAVP and conjugated estrogens for a recurrent large subcutaneous hematoma in Ehlers-Danlos syndrome. Am J Hematol 72:71–72.

Yeowell H, Steinmann B., 2008. Ehlers-Danlos syndrome, kyphoscoliotic form. In: GeneReviews at genetests: Medical Genetics Information Resource (database online).Copyright, University of Washington, Seattle 1997–2009. Available at http: //www.genetests.org. Accessed January 23, 2010.

CHN1 Mutations Are Not a Common Cause of Sporadic Duane's Retraction Syndrome

Noriko Miyake,[1,2] Caroline Andrews,[1,3,4] Wen Fan,[5] Wei He,[1] Wai-Man Chan,[1,4] and Elizabeth C. Engle[1,2,3,4,5,6,7,8,9]*

[1]Department of Neurology, Children's Hospital Boston, Boston, Massachusetts

[2]Department of Medicine (Genetics), Children's Hospital Boston, Boston, Massachusetts

[3]Department of Neurology, Harvard Medical School, Boston, Massachusetts

[4]Howard Hughes Medical Institute, Chevy Chase, Maryland

[5]Program in Neuroscience, Harvard Medical School, Boston, Massachusetts

[6]Department of Ophthalmology, Children's Hospital Boston, Boston, Massachusetts

[7]FB Kirby Neurobiology Center, Children's Hospital Boston, Boston, Massachusetts

[8]Program in Genomics, Children's Hospital Boston, Boston, Massachusetts

[9]Manton Center for Orphan Disease Research, Children's Hospital Boston, Boston, Massachusetts

TO THE EDITOR:

Duane retraction syndrome (DRS) is a congenital disorder characterized by restricted horizontal eye movement with globe retraction and palpebral fissure narrowing on attempted adduction. DRS is observed in ~0.1% of the general population, accounts for 1–5% of all strabismus [Kirkham, 1970; DeRespinis et al., 1993], and if untreated in childhood can result in loss of binocular vision and amblyopia. Postmortem examinations of individuals with sporadic DRS have revealed absence of the abducens motor neurons and abducens cranial nerve on the affected side(s), and aberrant innervation of the lateral rectus by axons of the oculomotor nerve that normally innervate the medial rectus muscle [Hotchkiss et al., 1980; Miller et al., 1982].

Most individuals with DRS are affected unilaterally and have no family history of the disorder [Kirkham, 1970]. Approximately 10% of individuals have a positive family history, however, and most of these individuals are bilaterally affected and segregate DRS as an autosomal-dominant trait. In addition, a quarter to half of affected individuals have syndromic DRS, with additional congenital defects most typically involving ocular, skeletal, auricular, or neuronal structures [Pfaffenbach et al., 1972]. These additional findings can co-segregate within DRS families and led to the identification of *SALL4* mutations in patients with DRS and radial ray anomalies (DRRS; OMIM 607323) [Al-Baradie et al., 2002; Kohlhase et al., 2002], and *HOXA1* mutations in patients with DRS, facial weakness, deafness, hypoventilation, vascular and cardiac outflow anomalies, and developmental delay/autism (OMIM 601536) [Tischfield et al., 2005]. Neither of these genes was found to be mutated in isolated, sporadic DRS [Wabbels et al., 2004; Tischfield et al., 2006].

We recently identified *CHN1* as the disease gene at the autosomal-dominant DURS2 locus on chromosome 2 [Miyake et al., 2008]. This is the only locus for nonsyndromic DRS mapped by linkage analysis, and four pedigrees had been reported to map to this location [Appukuttan et al., 1999; Evans et al., 2000; Engle et al.,

215

TABLE I. *CHN1* Single-Nucleotide Variants Observed Among DRS Probands

No. of probands with variant	Location of change[a]	Amino acid substitution	dbSNP reference ID	No. of controls with variant
1	1-35G>T, 5'UTR	None	None	0/213
1	261-24A>T, intron 5	None	None	1/187
1	588C>T, exon7	E196E	None	0/264
1	886+15G>A, intron 9	None	rs12613075	
2	964+54A>G, intron 10	None	None	0/285
3	964+123A>T, intron 10	None	rs56694150	
6	965-100G>A, intron 10	None	rs57776382	

[a]Nucleotide numbering refers to the cDNA sequence specifying the 1,380 amino acid residues of *CHN1* alpha2-chimerin splice form, commencing at the +1 position of the initiation codon [NM_001822].

2007]. We analyzed these four pedigrees as well as additional families segregating DRS as an autosomal-dominant trait and identified seven different causative heterozygous missense mutations in seven pedigrees [Miyake et al., 2008]. Notably, in comparison to individuals with sporadic DRS, the affected members of these families had a higher incidence of bilateral DRS and of vertical movement abnormalities. In addition, magnetic resonance imaging revealed hypoplasia of the oculomotor as well as the abducens nerve [Demer et al., 2007, #3090]. *CHN1* encodes alpha2-chimerin, a Rac guanosine triphosphatase-activating protein (RacGAP). We demonstrated that the seven DRS *CHN1* missense mutations increase the activity of alpha2-chimerin, lower Rac-GTP levels in the cell, and result in failure of oculomotor axons to innervate their target extraocular muscles in the developing chick embryo [Miyake et al., 2008].

To determine whether *CHN1* mutations are a common cause of sporadic DRS, we have now reviewed all probands enrolled in our genetic study of complex strabismus and identified 140 DRS probands with a negative family history for DRS. This study was prospectively reviewed and approved by the Children's Hospital Boston Office of Clinical Investigations, and informed consent was obtained from all participants and/or their guardians. Ophthalmological and general examinations were either performed at Children's Hospital Boston or obtained from the proband's medical record. Each participant provided a salivary or blood sample for DNA extraction.

The 140 probands were of diverse ethnicity and from diverse geographic locations, including North, Central, and South America, Europe, Middle East, Asia, India, and Australia. Of these, 36 had additional congenital anomalies and 6 had known chromosomal abnormalities not overlapping with the DURS2 locus. Detailed ophthalmological data were available from 90 probands and, of these, 72% had DRS type 1, 20% had DRS type 3, and 8% had DRS type 2 as per the Huber classification [1974]. In addition, 86% had unilateral DRS and, of these, 73% were left-sided. Of the 18 individuals with bilateral DRS, 5 had associated nonocular findings. Overall, the clinical features of the cohort correspond to other cohorts in the literature [DeRespinis et al., 1993].

We screened DNA extracted from blood or saliva from the 140 probands for sequence variants in the 13 coding exons and exon–intron boundaries of the *CHN1* gene (primer sequences

available on request). Amplicons were analyzed through a combination of denaturing high-performance liquid chromatography (dHPLC) (WAVE; Transgenomic, Inc., Omaha, NE) and direct sequencing as previously reported [Miyake et al., 2008]. Each variant detected by dHPLC was sequenced.

No *CHN1* mutations were detected in any of the 140 DRS probands. We did detect seven heterozygous single-nucleotide substitutions (Table I), of which three are known polymorphisms (SNPs) and a fourth, 261-24A>T in intron 5, we found in 1 of 187 controls of mixed ethnicity. Although we did not detect the remaining three variants (1-35G>T in the 5'UTR, 588C>T in exon 7, and 964+54A>G in intron 10) on 420 control alleles of mixed ancestry screened by dHPLC, only 588C>T is in coding sequence and it results in a synonymous amino acid substitution (E196E), and none are predicted to be promoter/enhancer regions or to alter splicing by either ESE finder 3.0 (http://rulai.cshl.edu/cgi-bin/tools/ESE3/esefinder.cgi), or splice site prediction by neural network from Berkeley Drosophila Genome Project (http://www.fruitfly.org/seq_tools/splice.html). Thus, these are most likely rare polymorphisms and not disease-causing.

The absence of *CHN1* coding mutations in 140 individuals with sporadic DRS is in contrast to the 35% detection rate of *CHN1* mutation in familial DRS (7/20 pedigrees) [Miyake et al., 2008]. There are several possible explanations for this discrepancy. The individuals harboring *CHN1* mutations identified to date were from families that segregate autosomal-dominant isolated DRS with a high incidence of bilateral involvement and additional abnormalities of vertical gaze. Only 13 of the 90 well-defined probands with sporadic DRS screened in this study had bilateral DRS in the absence of additional anomalies, and only 1 of the 13 had additional vertical gaze abnormalities noted. Thus, it is possible that the de novo *CHN1* mutation rate is low and our cohort contained too few individuals with sporadic, isolated, nonsyndromic DRS to detect new mutations. We have not, however, eliminated the possibility that individuals with sporadic DRS harbor somatic *CHN1* mutations that were not present in the saliva and/or lymphocytes from which their DNA was obtained. It is also possible that these individuals have an extra copy of *CHN1* or harbor mutations in undefined *CHN1* regulatory regions that we did not sequence, either of which could result in gain-of-function of the alpha2-chimerin protein and, hence, the DURS2 phenotype.

If *CHN1* gain-of-function mutations simply cause a rare variant form of DRS and we are not missing somatic or germ-line *CHN1* mutations, what causes the common sporadic form of this disorder? Although we are not aware of families segregating DRS that are large enough for informative linkage analysis and do not harbor *CHN1* mutations, only 35% of the dominant pedigrees we reported harbor *CHN1* mutations, supporting the presence of additional genetic causes of DRS in small families and potentially sporadic cases. Some sporadic cases may represent autosomal-recessive transmission and, consistent with this possibility, four probands in the current cohort are offspring of closely related parents. It is also interesting that there are several reports of individuals with sporadic DRS and chromosomal anomalies [Cullen et al., 1993; Pizzuti et al., 2002], including four probands enrolled in this study, suggesting that de novo rearrangements or copy number variations may underlie a subset of DRS. Finally, some cases of sporadic DRS likely result from epigenetic and/or environmental factors. Indeed, prenatal exposure to thalidomide has been shown to cause DRS [Miller, 1991].

We conclude that *CHN1* mutations are not a major cause of DRS among individuals with sporadic disease. Based on our findings, we recommend *CHN1* mutation screening in individuals with isolated DRS that segregates as an autosomal-dominant trait. Among these families, we would hypothesize that those whose affected members have bilateral DRS and additional vertical movement abnormalities are most likely to be mutation positive.

ACKNOWLEDGMENTS

REFERENCES

Al-Baradie R, Yamada K, St Hilaire C, Chan WM, Andrews C, McIntosh N, Nakano M, Martonyi EJ, Raymond WR, Okumura S, Okihiro MM, Engle EC. 2002. Duane radial ray syndrome (Okihiro syndrome) maps to 20q13 and results from mutations in SALL4, a new member of the SAL family. Am J Hum Genet 71:1195–1199.

Appukuttan B, Gillanders E, Juo SH, Freas-Lutz D, Ott S, Sood R, Van Auken A, Bailey-Wilson J, Wang X, Patel RJ, Robbins CM, Chung M, Annett G, Weinberg K, Borchert MS, Trent JM, Brownstein MJ, Stout JT. 1999. Localization of a gene for Duane retraction syndrome to chromosome 2q31. Am J Hum Genet 65:1639–1646.

Cullen P, Rodgers CS, Callen DF, Connolly VM, Eyre H, Fells P, Gordon H, Winter RM, Thakker RV. 1993. Association of familial Duane anomaly and urogenital abnormalities with a bisatellited marker derived from chromosome 22. Am J Med Genet 47:925–930.

Demer JL, Clark RA, Lim KH, Engle EC. 2007. Magnetic resonance imaging evidence for widespread orbital dysinnervation in dominant Duan's retraction syndrome linked to the DURS2 locus. Invest Ophthalmol Vis Sci 481:194–202.

DeRespinis PA, Caputo AR, Wagner RS, Guo S. 1993. Duane's retraction syndrome. Surv Ophthalmol 38:258–288.

Engle EC, Andrews C, Law K, Demer JL. 2007. Two pedigrees segregating Duane's retraction syndrome as a dominant trait map to the DURS2 genetic locus. Invest Ophthalmol Vis Sci 48:189–193.

Evans JC, Frayling TM, Ellard S, Gutowski NJ. 2000. Confirmation of linkage of Duane's syndrome and refinement of the disease locus to an 8.8-cM interval on chromosome 2q31. Hum Genet 106:636–638.

Hotchkiss MG, Miller NR, Clark AW, Green WG. 1980. Bilateral Duane's retraction syndrome: A clinical-pathological case report. Arch Ophthalmol 98:870–874.

Huber A. 1974. Electrophysiology of the retraction syndrome. Br J Ophthalmol 58:293–300.

Kirkham T. 1970. Inheritance of Duane's syndrome. Br J Ophthalmol 54:323–329.

Kohlhase J, Heinrich M, Schubert L, Liebers M, Kispert A, Laccone F, Turnpenny P, Winter RM, Reardon W. 2002. Okihiro syndrome is caused by SALL4 mutations. Hum Mol Genet 11:2979–2987.

Miller M. 1991. Thalidomide embryopathy: A model for the study of congenital incomitant horizontal strabismus. Trans Am Ophthalmol Soc 89:623–674.

Miller NR, Kiel SM, Green WR, Clark AW. 1982. Unilateral Duane's retraction syndrome (type 1). Arch Ophthalmol 100:1468–1472.

Miyake N, Chilton J, Psatha M, Cheng L, Andrews C, Chan WM, Law K, Crosier M, Lindsay S, Cheung M, Allen J, Gutowski NJ, Ellard S, Young E, Iannaccone A, Appukuttan B, Stout JT, Christiansen S, Ciccarelli ML, Baldi A, Campioni M, Zenteno JC, Davenport D, Mariani LE, Sahin M, Guthrie S, Engle EC. 2008. Human CHN1 mutations hyperactivate alpha2-chimaerin and cause Duane's retraction syndrome. Science 321:839–843.

Pfaffenbach D, Cross H, Kearns T. 1972. Congenital anomalies in Duane's retraction syndrome. Arch Ophthalmol 88:635.

Pizzuti A, Calabrese G, Bozzali M, Telvi L, Morizio E, Guida V, Gatta V, Stuppia L, Ion A, Palka G, Dallapiccola B. 2002. A peptidase gene in chromosome 8q is disrupted by a balanced translocation in a duane syndrome patient. Invest Ophthalmol Vis Sci 43:3609–3612.

Tischfield MA, Bosley TM, Salih MA, Alorainy IA, Sener EC, Nester MJ, Oystreck DT, Chan WM, Andrews C, Erickson RP, Engle EC. 2005. Homozygous HOXA1 mutations disrupt human brainstem, inner ear, cardiovascular and cognitive development. Nat Genet 37:1035–1037.

Tischfield MA, Chan WM, Grunert JF, Andrews C, Engle EC. 2006. HOXA1 mutations are not a common cause of Duane anomaly. Am J Med Genet Part A 140A:900–902.

Wabbels BK, Lorenz B, Kohlhase J. 2004. No evidence of SALL4-mutations in isolated sporadic duane retraction "syndrome" (DURS). Am J Med Genet Part A 131A:216–218.

ARTICLE

SMOC1 Is Essential for Ocular and Limb Development in Humans and Mice

Ippei Okada,[1,14] Haruka Hamanoue,[1,2,14] Koji Terada,[3] Takaya Tohma,[4] Andre Megarbane,[5] Eliane Chouery,[5] Joelle Abou-Ghoch,[5] Nadine Jalkh,[5] Ozgur Cogulu,[6] Ferda Ozkinay,[6] Kyoji Horie,[7] Junji Takeda,[7,8] Tatsuya Furuichi,[9,10] Shiro Ikegawa,[9] Kiyomi Nishiyama,[1] Satoko Miyatake,[1] Akira Nishimura,[1] Takeshi Mizuguchi,[1,15] Norio Niikawa,[11,12] Fumiki Hirahara,[2] Tadashi Kaname,[13] Koh-ichiro Yoshiura,[12] Yoshinori Tsurusaki,[1] Hiroshi Doi,[1] Noriko Miyake,[1] Takahisa Furukawa,[3] Naomichi Matsumoto,[1,*] and Hirotomo Saitsu[1,*]

Microphthalmia with limb anomalies (MLA) is a rare autosomal-recessive disorder, presenting with anophthalmia or microphthalmia and hand and/or foot malformation. We mapped the MLA locus to 14q24 and successfully identified three homozygous (one nonsense and two splice site) mutations in the SPARC (secreted protein acidic and rich in cysteine)-related modular calcium binding 1 (*SMOC1*) in three families. *Smoc1* is expressed in the developing optic stalk, ventral optic cup, and limbs of mouse embryos. *Smoc1* null mice recapitulated MLA phenotypes, including aplasia or hypoplasia of optic nerves, hypoplastic fibula and bowed tibia, and syndactyly in limbs. A thinned and irregular ganglion cell layer and atrophy of the anteroventral part of the retina were also observed. Soft tissue syndactyly, resulting from inhibited apoptosis, was related to disturbed expression of genes involved in BMP signaling in the interdigital mesenchyme. Our findings indicate that SMOC1/Smoc1 is essential for ocular and limb development in both humans and mice.

Introduction

Microphthalmia with limb anomalies (MLA [MIM 206920]), also known as Waardenburg anophthalmia syndrome or ophthalmoacromelic syndrome, is a rare autosomal-recessive disorder first described by Waardenburg.[1] It is characterized by ocular anomalies ranging from mild microphthalmia to true anophthalmia and by limb anomalies such as oligodactyly, syndactyly, and synostosis of the 4th and 5th metacarpals.[2–4] The genetic cause for MLA has remained unknown.

It is widely known that secreted signaling molecules such as Sonic hedgehog (Shh), wingless-type MMTV integration site family (Wnt), transforming growth factor β (Tgf-β), bone morphogenetic proteins (Bmps), and fibroblast growth factor (Fgf) are involved in the development of many organs and tissues, including the eyes and limbs.[5,6] In particular, mutations in *BMP4* (MIM 112262) have resulted in anophthalmia with systemic manifestations, including polydactyly and/or syndactyly (also known as micropthalmia, syndromic 6, MCOPS6 [MIM

607932]),[7] highlighting importance of BMP signaling in both the developing eye and limb.

SMOC1 (MIM 608488), which encodes SPARC (secreted protein acidic and rich in cysteine)-related modular calcium binding 1, is a member of the SPARC (also known as BM-40) matricellular protein family that modulates cell-matrix interaction by binding to many cell-surface receptors, the extracellular matrix, growth factors, and cytokines.[8,9] SMOCs are extracellular glycoproteins with five domains: an N-terminal follistatin-like (FS) domain, two thyroglobulin-like (TY) domains, a domain unique to SMOC, and an extracellular calcium-binding (EC) domain.[9] SMOC1 is widely expressed in various tissues with localization to basement membranes.[9,10] Although the biological function of SMOC1 remains largely unknown, it has been recently reported that *Xenopus* smoc protein, the ortholog of human SMOC1, acts as a BMP antagonist,[11] suggesting that human SMOC1 can also modulate BMP signaling.

Here, we demonstrate that *SMOC1* mutations cause MLA. We also show that *Smoc1* null mice recapitulated

[1]Department of Human Genetics, Yokohama City University Graduate School of Medicine, 3-9 Fukuura, Kanazawa-ku, Yokohama 236-0004, Japan; [2]Department of Obstetrics and Gynecology, Yokohama City University Graduate School of Medicine, 3-9 Fukuura, Kanazawa-ku, Yokohama 236-0004, Japan; [3]Department of Developmental Biology, Osaka Bioscience Institute, 6-2-4 Furuedai, Suita, Osaka 565-0874, Japan; [4]Division of Pediatrics, Okinawa Prefectural Nanbu Medical Center & Children's Medical Center, 118-1 Ikyoku, Arakawa, Haebaru, Okinawa 901-1193, Japan; [5]Medical Genetics Unit, St. Joseph University, Beirut 1104-2020, Lebanon; [6]Department of Pediatrics, Ege University Faculty of Medicine, 35100 Bornova-Izmir, Turkey; [7]Department of Social and Environmental Medicine, Graduate School of Medicine, Osaka University, 2-2 Yamadaoka, Suita, Osaka 565-0871, Japan; [8]Center for Advanced Science and Innovation, Osaka University, 2-1 Yamadaoka, Suita, Osaka 565-0871, Japan; [9]Laboratory for Bone and Joint Disease, Center for Genomic Medicine, RIKEN, 4-6-1 Shirokanedai, Minato-ku, Tokyo 108-8639, Japan; [10]Laboratory Animal Facility, Research Center for Medical Sciences, Jikei University School of Medicine, 3-25-8, Nishi-Shimbashi, Minato-ku, Tokyo 105-8461, Japan; [11]Research Institute of Personalized Health Sciences, Health Sciences University of Hokkaido, Ishikari-Tobetsu, Hokkaido 061-0293, Japan; [12]Department of Human Genetics, Nagasaki University Graduate School of Biomedical Sciences, Sakamoto 1-12-4, Nagasaki 852-8523, Japan; [13]Department of Medical Genetics, University of the Ryukyus Faculty of Medicine, 207 Uehara, Nishihara, Okinawa 903-0215, Japan
[14]These authors contributed equally to this work
[15]Current address: Laboratory of Biochemistry and Molecular Biology, National Cancer Institute, National Institutes of Health, Building 37, Room 6050, Bethesda, MD 20892, USA
*Correspondence: naomat@yokohama-cu.ac.jp (N.M.), hsaitsu@yokohama-cu.ac.jp (H.S.)

48

MLA phenotypes, indicating that *SMOC1* plays essential roles in both eye and limb development in humans and mice.

Subjects and Methods

Subjects

A total of four families with one or two cases of MLA were analyzed in this study, including three previously reported families (A, B, and C).[12,13] Family X from Turkey, which has been previously described,[14] was newly recruited to this study. Detailed clinical information of all the patients is available in the literature,[12,14] and phenotypes of patients with confirmed mutations are summarized in Table S1 (available online). A total of five affected and 16 unaffected members from the four families were analyzed in the linkage study. Genomic DNA was obtained from peripheral-blood leukocytes with the use of QuickGene 610-L (Fujifilm, Tokyo, Japan) after informed consent had been given. Experimental protocols were approved by the institutional review board of Yokohama City University School of Medicine.

SNP Genotyping, and Fine Mapping with Short Tandem Repeat Markers

Whole-genome SNP genotyping, with the use of GeneChip Human Mapping 50K Array XbaI (Affymetrix, Santa Clara, CA), and fine mapping of possible candidate regions, with the use of additional microsatellite markers, were performed as previously described.[12,15] The list of primers used for fine mapping is presented in Table S2.

Linkage Analysis

Multipoint linkage analyses using aligned SNPs were performed with ALLEGRO software.[16] Two-point linkage analyses of candidate regions were performed with the LINKAGE package MLINK (FASTLINK software, version 5.1). In each program, an autosomal-recessive model of inheritance with complete penetrance and a disease-allele frequency of 0.001 were applied.

Mutation Analysis of Candidate Genes

All coding exons and exon-intron boundaries of *RAD51L1* (MIM 602948), *ACTN1* (MIM 102575), *ERH* (MIM 601191), *SRSF5* (MIM 600914), *DCAF5* (MIM 603812), *COX16*, *EXD2*, *GALNTL1*, *SLC39A9*, *KIAA0247*, *MED6* (MIM 602984), *TTC9* (MIM 610488), *MAP3K9* (MIM 600136), and *SMOC1* (transcript variant 1, GenBank accession number NM_001034852.1) were analyzed in the probands of families A, C, and X. The transcript variant 2 of *SMOC1* (GenBank accession number NM_022137.4) is 3 bp shorter than the variant 1, leading to an in-frame amino acid deletion at position 431. PCR was cycled 35 times at 94°C for 30 s, at 60°C for 30 s, and at 72°C for 30–90 s in a total volume of 20 μl containing 30 ng genomic DNA as a template, 0.5 μM forward and reverse primers, 200 μM each deoxyribonucleotide triphosphate (dNTP), 1 × ExTaq buffer, and 0.25 U ExTaq (Takara). All primers were designed with Primer3 software. Detailed information of primers is available upon request. PCR products were purified with ExoSAP (USB) and sequenced with BigDye Terminator 3.1 (Applied Biosystems) on a 3100 Genetic Analyzer. Sequences of patients were compared to reference genome sequences in the UCSC Genome Browser (February 2009 assembly) with Seqscape software, version 2.1 (Applied Biosystems).

Animals

Smoc1 mutant mice, created with the use of the *Sleeping Beauty* transposon system, have been previously described.[17] Line PV384 was provided by the RIKEN BioResource Center through the National BioResource Project of MEXT, Japan. Three independent mouse lines (no. 1 to no. 3), each with a single insertion in intron 1 of *Smoc1*, were bred as heterozygotes. Lines 1 and 3 were backcrossed for at least four generations to a C57BL/6J background. Line 2 was maintained with a mixed background of C57BL/6J and ICR. We mainly analyzed line 1, but we confirmed similar phenotypes in lines 2 and 3. Animals were housed in accordance with protocols approved by the Institutional Animal Care and Use Committee at Yokohama City University, School of Medicine. PCR genotyping of mice was performed with the use of genomic DNA from yolk-sac, ear, or tail biopsies. The following primers were used: PV384-WF, 5′-AAAGGCTGGGAATTGTTTG A-3′; PV384-WR, 5′-TGCAGCTGAAACTGTCTCTCC-3′; PV384-MF, 5′-TGTCCTAACTGACTTGCCAAA-3′. The PV384-WF/PV384-WR primers amplified a 441 bp wild-type (WT) product, and the PV384-MF/PV384-WR primers amplified a 218 bp mutant product.

Southern Hybridization

Genomic DNA was extracted from livers or tail biopsies of PV384 heterozygous (*Smoc1^Tp/+*) mice via standard protocols. The gene-trap insertions were analyzed by Southern hybridization with the use of 10 μg of SacI-, NdeI-, BglII-, and EcoRI-digested DNA. The probe (451 bp), which hybridized to the internal ribosome entry site (IRES) in the gene-trap vector, was synthesized with the DIG PCR Probe Synthesis Kit (Roche) with the use of the following primers: 5′-CTAACGTTACTGGCCGAAGC-3′ and 5′-CCCAGATCAGATCCCATACAA-3′. Hybridization, washing, and detection of probes were performed according to the manufacturer's protocol. Images were captured with the FluorChem system (Alpha Innotech).

Cloning of Gene-Trap Insertion Sites

After identification of aberrant DNA fragments by Southern hybridization, NdeI-, SacI-, and EcoRI-digested DNA from PV384 mice was fractionated by electrophoresis, and appropriately sized fragments containing *Ol1* (*other locus 1*), *Ol2*, and *Ol3* were isolated with a QIAEXII Gel Extraction Kit (QIAGEN). The isolated DNA was self-ligated by Ligation High ver.2 (Toyobo), precipitated with ethanol, and dissolved in 20 μl EB buffer (QIAGEN). Inverse PCR was performed in 25 μl reactions, containing 2 μl ligated DNA, 1 × PCR buffer for KOD FX, 0.4 mM each dNTP, 0.5 μM each primer, and 0.5 U KOD FX DNA polymerase (Toyobo). Primers common to *Ol1*, *Ol2*, and *Ol3* were as follows: Inv-F, 5′- AT CGCCAGTTCTGTATGAACGGTCTGGTCTT-3′; Inv-R, 5′-CCCTC TTTACGTGCCAGCCATCTTAGAGATAC-3′. Confirmatory PCR of gene-trap insertion sites for *Ol1*, *Ol2*, and *Ol3* loci was performed with the use of the following primers: *Ol1*-F, 5′-GAGTGGTATTCA TTGGATTCTGCTGAT-3′; *Ol2*-F, 5′-AAATCCAGCTGGCCAACAGA CTAAG-3′; *Ol3*-F, 5′-TTGCCGGGTAGACTCTATCAAGAACCA-3′; TBAL-R, 5′-CTTGTGTCATGCACAAAGTAGATGTCC-3′. Primer sets of *Ol1*-F/TBAL-R, *Ol2*-F/TBAL-R, and *Ol3*-F/TBAL-R could amplify 175 bp, 607 bp, and 767 bp products, respectively. These PCR primer pairs were also used for genotyping of mice harboring a single insertion at the *Smoc1* locus.

49

Confirmation of Promoter- and Poly(A)-Trapped Transcripts

Whole embryos at embryonic day 10.5 (E10.5) and E11.5 were stored in RNAlater solution (QIAGEN). Total RNA was extracted from WT, $Smoc1^{Tp/+}$, and $Smoc1^{Tp/Tp}$ embryos with the use of RNeasy Plus Mini (QIAGEN). One microgram total RNA was subjected to reverse transcription with the use of a PrimeScript 1st Strand Synthesis Kit with random hexamers (Takara). A control reaction with no reverse transcriptase was included in each experiment. PCR was performed in 20 μl reactions, containing 1 μl cDNA, 1 × PCR Buffer for KOD FX, 0.4 mM each dNTP, 0.3 μM each primer, and 0.4 U KOD FX (Toyobo). Primers used are listed below: Smoc1-F, 5′-GTCCCCACCTCCCCAAGTGCTTTGA-3′; LacZ-R, 5′-TGCCAAAAGACGGCAATATGGTGGAAA-3′; GFP-F, 5′-TCACATGGTCCTGCTGGAGTTCGTGAC-3′; Smoc1-R, 5′-ACACTTGCTCTGGCCAGCATCTTTGCAT-3′. Primer sets of Smoc1-F/Smoc1-R, Smoc1-F/LacZ-R, and GFP-F/Smoc1-R could amplify native Smoc1 (366 bp), promoter-trapped transcripts (Tp-LacZ, 500 bp) and poly(A)-trapped transcripts (Tp-GFP, 308 bp), respectively. The PCR conditions were 98°C for 10 s, 68°C for 1 min, for 30 cycles. Primers for ACTB[18] were used as an internal control. PCR for ACTB was cycled 20 times at 94°C for 20 s, 60°C for 20 s, and 72°C for 30 s in a total volume of 10 μl containing 0.5 μl cDNA, 0.4 μM each primer, 0.2 mM each dNTP, 1 × ExTaq buffer, and 0.5 U ExTaq HS (Takara). All PCR products were electrophoresed on 2% agarose gels.

In Situ Hybridization

Embryos were collected between E9.5 and E13.5. Whole-mount in situ hybridization was carried out as previously described.[19,20] Two fragments of Smoc1 cDNA were obtained as probes by RT-PCR, with the use of total RNA extracted from livers of E16.5 mouse embryos, and subcloned into pCR4-TOPO (Invitrogen). Primer sequences were as follows: probe 1-F, 5′-GTCTGCTCACGCCCCACT-3′; probe 1-R, 5′-CCTGAACCATGTCTGTGGTG-3′; probe P-F, 5′-CAGGAACAGGAAAGGGAAGA-3′; probe P-R, 5′-AAGGGAAAACCACACAGCAC-3′. PCR products were 1023 bp and 1578 bp, corresponding to nucleotide positions 275–1297 and 1849–3426 of the mouse Smoc1 cDNA (GenBank accession number NM_001146217.1), respectively. The cDNA fragment amplified with probe P-F and probe P-R primers was identical to the probe used in a previous report.[21] Digoxigenin-labeled sense and antisense riboprobes were synthesized with the use of a digoxigenin RNA labeling kit (Roche). These two different antisense probes demonstrated identical staining patterns, and the control sense probes showed no staining. The expression pattern was confirmed with more than three embryos. In addition, the following probes were used: Bmp2 (gift from Y. Takahashi),[22] Sox9 (gift from A. Yamada),[22] Bmp7 (gift from E.J. Robertson), and Msx2 (gift from Dr. R.E. Maxson, Jr). The numbers of embryos examined were as follows (numerical quantity for WT, $Smoc1^{Tp/+}$, and $Smoc1^{Tp/Tp}$, respectively, shown in parentheses): Msx2 (2, 1, 3) at E11.5; Bmp2 (3, 0, 3), Bmp7 (3, 0, 3), Msx2 (3, 0, 3), and Sox9 (2, 1, 3) at E12.5; Bmp2 (1, 2, 3), Bmp7 (2, 1, 3), Msx2 (1, 2, 3), and Sox9 (1, 3, 4) at E13.5. Stained embryos were cleared in glycerol to enable images to be produced with a VHX-1000 digital microscope (Keyence).

Histology

Heads of embryos and newborns were fixed overnight in 4% paraformaldehyde in PBS at 4°C. These embryos were then washed in PBS. Frozen samples were serially sectioned at 16 μm (E14.5) and 20 μm (P0). The numbers of eyes examined (WT, $Smoc1^{Tp/+}$, $Smoc1^{Tp/Tp}$) were as follows: coronally sectioned at E14.5 (8, 10, 12), coronally sectioned at P0 (8, 10, 6), horizontally sectioned at P0 (2, 2, 4). For evaluation of ventral atrophy of the retina, only the coronally sectioned eyes were used. TB staining was performed according to standard protocols. Forelimbs of mice were fixed in 4% paraformaldehyde in PBS, decalcified in 10% EDTA, and embedded in paraffin. Forelimbs were serially sectioned at 4 μm and stained with hematoxylin and eosin.

Evaluation of Optic Nerve Diameter

The palatine and orbital bones were carefully removed to expose the optic chiasm and optic nerve. During the dissection process, 4% paraformaldehyde in PBS was frequently applied onto the gaps between the bone and optic nerve. Xylene cyanol was applied to enhance the outline of optic nerves at poastnatal day 0 (P0). Photographs of optic nerves were taken with a VHX-1000 digital microscope, and the diameter was measured for right and left optic nerves with the bundled software included with the VHX-1000 instrument.

Skeletal Staining

For skeletal preparations, mice were fixed in 99.5% ethanol after removal of the skin and viscera. Cartilage tissues were stained with 0.015% alcian blue and 20% acetic acid in 75% ethanol for three days at 37°C. After dehydration with 99.5% ethanol for three days, bones were stained with 0.002% alizarin red in 1% KOH. Then skeletons were cleared in 1% KOH for several weeks. For P14 mice, soft tissues were dissolved in 2% KOH before alizarin red staining.

Nile Blue Staining

For the study of apoptosis of hindlimbs at E13.5 and E14.5, Nile blue (NB) staining was performed on the basis of a previously described protocol,[23] except that staining was performed at 37°C (not room temperature). Apoptosis was determined by NB-stained (deceased) cells. After rinsing in Tyrode solution, hindlimbs of control (WT and heterozygous littermates) and homozygous mice were evaluated. Photographs of dorsal aspects were taken with a VHX-1000 digital microscope. Experiments were repeated three times, and reproducible representative results are presented.

Statistical Analysis

Statistical analyses were performed with the use of non-repeated-measures ANOVA followed by Dunnett's post hoc test. The results are given as mean ± standard deviation, and the threshold p value for statistical significance was 0.01.

Results

Identification of Homozygous SMOC1 Mutations

We have previously mapped the MLA locus to a 422 kb region at 10p11.23 by analyzing three families (one Japanese family [A] and two Lebanese families [B and C]). This region contained only one gene, MPP7, in which no mutations were found.[12] After a new Turkish family (X) was added to the analysis, the MLA locus was again searched by homozygosity mapping to the consanguineous families (X, B, and C) and haplotype mapping to family A for detection of compound-heterozygous mutations; however, we could not detect any common regions

among the four families. We then focused on identifying common regions in any three of the four families to allow for locus heterogeneity (Table S3).

A locus at 14q24.1-q24.2, which showed the highest LOD score (3.936) among the candidate regions larger than 2.0 Mb, was highlighted among families A, C, and X. This locus was analyzed with the use of additional microsatellite markers, and a 3.0 Mb region containing 24 genes was identified (Figures 1A and 1B). A total of 14 genes were sequenced, and homozygous mutations were found in SMOC1: c.718C>T (p.Gln240X) in family A, c.664+1G>A in family C, and c.378+1G>A in family X (Figures 1C and 1D). All of these homozygous mutations were cosegregated with the disease phenotype, and the parents of the individuals with these mutations were heterozygous carriers (Figure 1C). We could not find any mutations in SMOC1 in family B, in which MLA is unlinked to the 14q24.1-q24.2 locus. Interestingly, in family A haplotypes of paternal and maternal alleles, each having the same mutation, are completely different (data not shown), suggesting that the same mutation may have occurred in separate events. The c.718C>T mutation was not detected in 289 healthy Japanese controls, including 100 Okinawa islanders. The other two mutations were not detected in ethnically matched controls (54 Lebanese and 99 Turkish subjects, respectively), nor in 289 Japanese controls. The two splice-donor-site mutations (c.664+1G>A and c.378+1G>A) are predicted to abolish a donor site, as predicted by ESE-finder, NetGene2, HSF2.4.1, SpliceView, and BDGP analysis (Table S4). Thus, the three mutations are likely to lead to a loss of functional SMOC1.

Smoc1 Expression in the Developing Eye and Limb in Mice

For the examination of Smoc1 expression in the developing eye and limb, whole-mount in situ hybridization of mouse embryos was performed. Smoc1 was expressed in the forebrain, midbrain, hindbrain, pharyngeal arch, somites, and forelimb buds at E9.5 (Figure 2A). At E10.5, Smoc1 expression was observed in the optic stalk (Figure 2B), and at E11.5, expression was localized to the closure site of the optic cup (Figure 2C). Expression of Smoc1 in developing limbs between E10.5 and E11.5 was observed in both dorsal and ventral regions, with a broader pattern of expression in dorsal regions, but expression was not detected in the most anterior, posterior, and distal parts of limb buds (Figures 2D and 2E). Expression coinciding with chondrogenic condensation was observed at E12.5 (Figure 2F), and expression then became restricted to future synovial joint regions at E13.5 (Figure 2G). This dynamic expression suggests that Smoc1 plays a critical role in ocular and limb development.

Ocular and Limb Anomalies in Smoc1 Null Mice

To investigate the pathological basis of MLA due to the loss of SMOC1 function, we obtained Smoc1 mutant mice, PV384.[17] PV384 mice possess gene-trap insertions in the Smoc1 locus and in three other loci. After PV384 mice were bred with C57BL/6J or ICR mice, we obtained three independent lines (no. 1 to no. 3), each with a sole insertion in intron 1 of Smoc1 (Figure S1). We mainly analyzed line 1, but we confirmed similar phenotypes in lines 2 and 3. Heterozygous mutant mice (Smoc1[TP/+]) were healthy and fertile. Homozygous mice (Smoc1[TP/TP]) were null mutants, as they showed no native transcript of Smoc1 (Figure S1E). Homozygous mice were viable at P0; however, they did not survive beyond the first 3 wks of life (Figure 3B). Their growth was retarded in comparison to WT and heterozygous littermates at P0 and P14 (Figures 3A and 3C). Developmental defects in eyes and optic nerves were evident at E14.5. Homozygous mice had relatively small eyes, and histological examinations revealed aplasia or hypoplasia of optic nerves (in 10 of 12 optic nerves), atrophy of the anteroventral part of the retina (in 11 of 12 eyes), and extension of the retinal pigmented epithelium (RPE) to the optic nerve (in 10 of 12 eyes) (Figures 3D–3I). These abnormalities were also observed at P0 (aplasia or hypoplasia of optic nerves [in 7 of 10 optic nerves], retinal atrophy [in 6 of 6 eyes], and RPE extension [in 3 of 6 eyes with identifiable optic nerves]) (Figures 3J–3M). WT or heterozygous littermates did not show any such abnormalities, except that a few eyes of heterozygous mice showed extension of the RPE at E14.5, but not at P0 (in 2 of 10 and 0 of 12 eyes, respectively). Toluidine blue (TB) staining showed ganglion cell layers that were thinned and irregular to varying degrees in homozygous mice, suggesting a reduced number of retinal ganglion cells (Figures 3J–3K′). Thus, Smoc1 is required for axon sprouting, elongation, or maintenance of retinal ganglion cells.[24] Hypoplasia of optic nerves was further quantitatively confirmed by macroscopic examination: the average diameter of optic nerves of homozygous mice was significantly smaller than that of WT and heterozygous littermates at P0 and P14 (Figures 3L–3Q). These data clearly demonstrate that loss of Smoc1 in mice affects development of the body, retina, and optic nerves, in a manner similar to that seen in MLA patients.[3,4]

Newborn homozygous mice could be readily identified by their hindlimb syndactyly and pes valgus, whereas no abnormalities were observed in WT and heterozygous pups (Figure 4 and Table 1). Interestingly, the severity of syndactyly varied between mouse lines: line 1 exclusively showed soft tissue syndactyly, whereas line 2 frequently showed four digits (Figures 4F and 4J). Skeletal preparations with alcian blue and alizarin red revealed that the foot with four digits had four phalanx and five metatarsals with fusion to each other (Figure 4K). Thus the Smoc1 null mutation resulted in a spectrum of phenotypes, from soft tissue syndactyly to four fused digits, probably due to different genetic backgrounds. Bowed tibiae and hypoplastic fibulae were also consistently observed in homozygous mice (Figures 4H and 4L). The articulation between
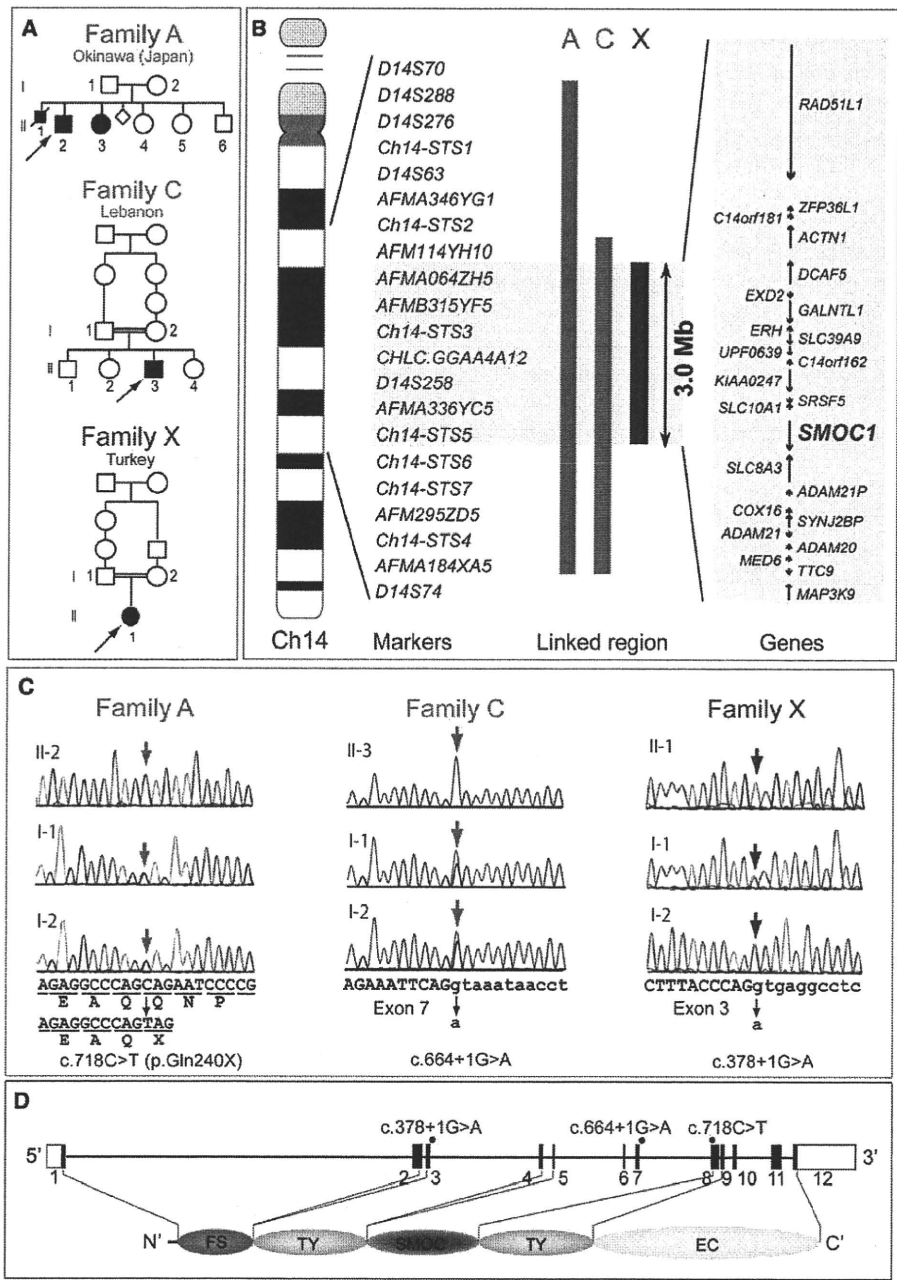
Figure 1. Genetic Analysis of Three Families with Members Affected by Microphthalmia with Limb Anomalies

(A) Pedigrees of the three families.

(B) Linkage analysis with SNPs and microsatellite markers on chromosome 14. From left to right: chromosome ideogram, genetic markers, linked regions of the three families, and genes mapped to the shortest overlapping linked region (between *AFM114YH10* and *Ch14-STS6* [UCSC coordinates, Feb. 2009: chromosome 14: 68,388,190–71,347,908 bp]).

(C) Sequences of mutations identified in each family. Affected patients in family A have a homozygous nonsense mutation (c.718C>T). Patients in families C and X have distinct homozygous splice-donor site mutations (c.664+1G>A and c.378+1G>A, respectively). For all mutations, parents of affected patients are heterozygous carriers, without exception. Sequences of the exon and intron are presented in upper and lower cases, respectively.

(D) At the top is a depiction of a schematic representation of *SMOC1* consisting of 12 exons (UTR and coding exons are indicated by open and filled rectangles, respectively). The locations of three mutations are indicated by red dots. At the bottom, the functional domains of SMOC1 are depicted. Abbreviations are as follows: FS, the follistatin-like domain; TY, the thyroglobulin-like domain; SMOC, the domain unique to SMOC; and EC, the extracellular calcium-binding domain.
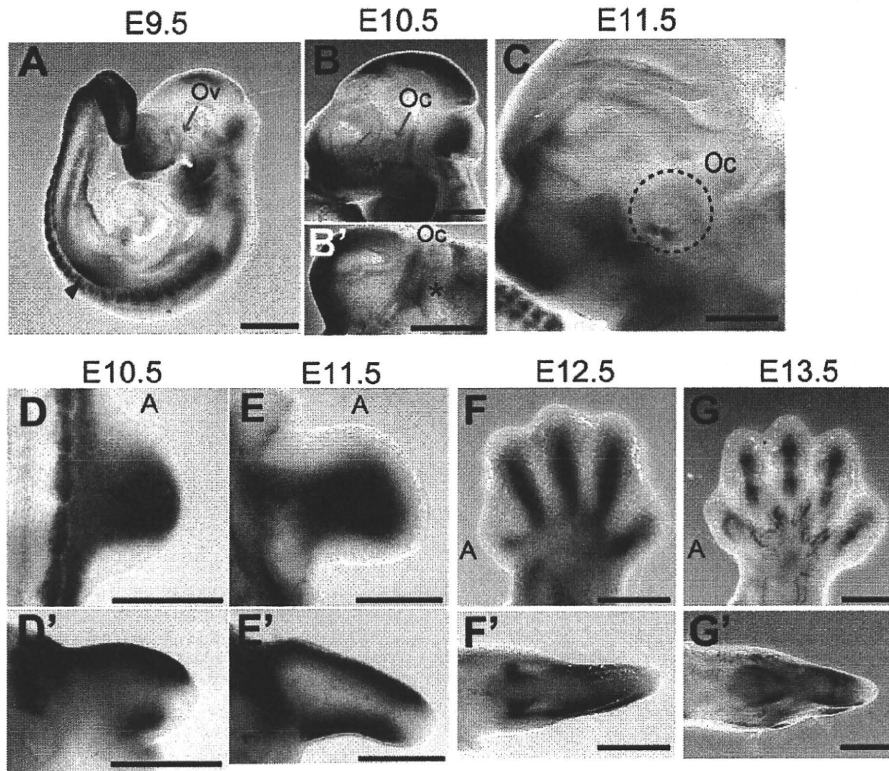
Figure 2. Smoc1 Expression in Mouse Embryos
Lateral views of embryos (A–C) and a ventral view of the left part of the head (B′, lateral view is shown at the top).
(A) At E9.5, *Smoc1* was expressed in the forebrain, midbrain, hindbrain, pharyngeal arch, somites, and forelimb buds (magenta arrowhead), but not in the optic vesicle (Ov, blue arrow).
(B and B′) Expression in the optic stalk became evident at E10.5 (magenta asterisks), but was not evident in the optic cup (Oc, blue arrow).
(C) Expression was restricted to the closure site of the optic cup (dashed circle) at E11.5.
(D–G) Dorsal and (D′–G′) posterior view of the right hindlimbs (dorsal view is shown at the top in D′–G′). The anterior side is indicated by an A. (D and D′) At E10.5, *Smoc1* was more widely expressed in the dorsal part of the limb bud than in the ventral part. *Smoc1* expression is undetected in the most anterior, posterior, and distal parts of the limb bud. (E and E′) At E11.5, ventral expression was broader than that in the previous stage. (F and F′) At E12.5, expression was detected in areas consistent with chondrogenic condensation. (G and G′) At E13.5, *Smoc1* expression became restricted to future joint regions. Scale bar represents 500 μm.

tibia/fibula and calcanea of homozygous mice appeared malpositioned (Figures 4G and 4K), which might contribute to pes valgus. At P14, soft tissue syndactyly was also evident in most forelimbs of homozygous mice (Figures 4M–4O). Moreover, hindlimbs of homozygous mice showed synostosis between the 4th and 5th metatarsals (Figure 4T), which is observed in both the hands and the feet of MLA patients. Thus, many limb anomalies of MLA patients were recapitulated in *Smoc1* null mice (Table S1).

Reduced Interdigital Apoptosis and Disturbed BMP Signaling

Among the various abnormalities caused by loss of *Smoc1* function, we focused on soft tissue syndactyly, which was commonly observed in both fore- and hindlimbs of null mutants. It is possible that the syndactyly is caused by failed apoptotic regression of the interdigital mesenchyme. To examine this hypothesis, hindlimbs were stained with NB sulfate at E13.5 and E14.5, the time

when interdigital apoptosis is most evident. In control embryos (WT and heterozygous littermates), NB-stained apoptotic cells were identified in the interdigital mesenchyme, where regression of the interdigital webbing occurs in the distal region (Figures 5A and 5C). By contrast, the number of apoptotic cells in the mesenchyme between digits 2 and 3 and digits 3 and 4 was dramatically reduced in homozygous mice at E13.5 and E14.5, along with persistent webbing in the distal region (Figures 5B and 5D, magenta asterisk). BMP signaling is involved in apoptosis of the interdigital mesenchyme.[25,26] *Bmp2*, *Bmp7*, and *Msx2*, a direct target of BMP signaling, were strongly expressed in the interdigital mesenchyme of control hindlimbs at both E12.5 and E13.5. However, the expression of these three genes was profoundly reduced and perturbed in hindlimbs of homozygous mice (Figures 5E–5J). These data suggest that inhibition of apoptosis is spatiotemporally correlated to reduced and/or disturbed expression of genes involved in BMP signaling in the interdigital mesenchyme.
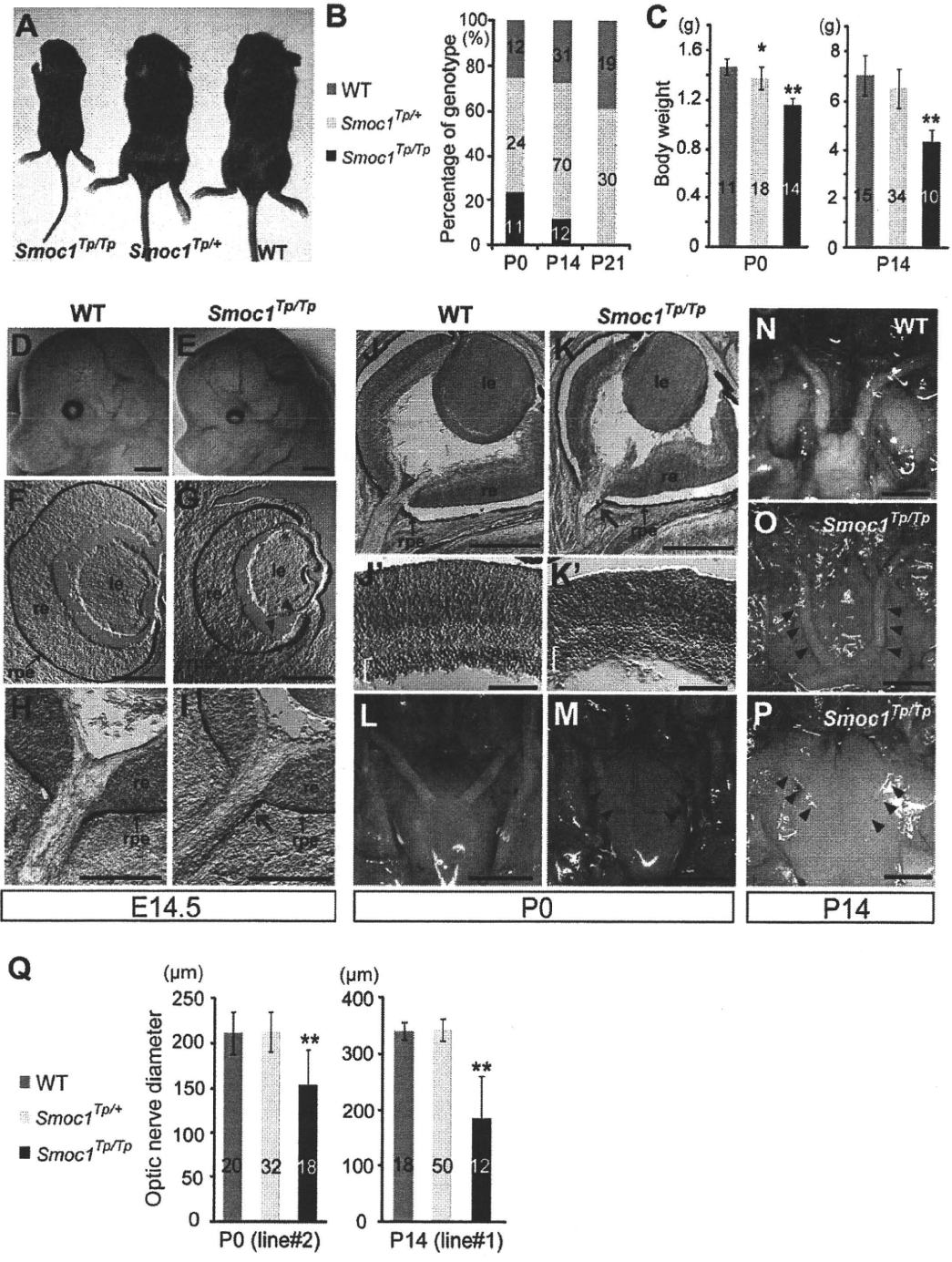
Figure 3. Growth and Ocular Phenotypes of *Smoc1* Null Mice
(A) Representative *Smoc1*[Tp/Tp] mouse, showing a small body in comparison to *Smoc1*[Tp/+] and WT littermates.
(B) Genotypes of living pups during the first 3 wk of life.
(C) Body weight of pups of each genotype at P0 (left panel) and P14 (right panel).
(D and E) Relatively small eyes were evident in *Smoc1*[Tp/Tp] mice in comparison to WT mice.
(F–K′) Coronal sections of eyes at E14.5 (F–I) and P0 (J–K′) with TB staining (H, I, and J–K′). (F-I) Atrophy of the anteroventral part of the retina (G, magenta arrowheads, dorsal view shown at the top), hypoplastic optic nerve, and extension of the RPE to the optic nerve (I, magenta arrow) in *Smoc1*[Tp/Tp] mice at E14.5. (J and K) Hypoplastic optic nerve and RPE extension in *Smoc1*[Tp/Tp] mice at P0 (K, magenta arrow). Note that sections in which optic nerves appeared most thick are presented in (H–K). (J′–K′) In higher-magnification views of (J and K), a thinned and irregular ganglion cell layer (white brackets) was observed in *Smoc1*[Tp/Tp] mice. Abbreviations are as follows: le, lens; re, retina; rpe, retinal pigmented epithelium.
(L–P) Ventral views of the brain showing optic nerves at P0 (L and M) and P14 (N–P), showing various degrees of optic nerve hypoplasia.

Discussion

In a previous report, we performed parametric linkage analysis with three families (families A, B, and C) and found 16 loci showing a LOD score ($\theta = 0.000$) higher than 3.0. Additional microsatellite markers highlighted only one locus, 10p11.23.[12] However, no mutations were found in the candidate gene *MPP7*.[12] By recruiting a new family (family X) to this study, we successfully found homozygous mutations in *SMOC1* in families A, C, and X. In family B, no *SMOC1* mutations were found, indicating the genetic heterogeneity in MLA. Patients with *SMOC1* mutations and *Smoc1* null mice showed similar limb anomalies, such as oligodactyly, syndactyly, synostosis of 4th and 5th metacarpals, hypoplasia of fibula, and bowed tibia. Oligodactyly, syndactyly, and synostosis of 4th and 5th metacarpals are common in MLA patients.[2–4] However, hypoplastic fibula and bowed tibia are less common in patients with MLA, as four out of 34 MLA patients showed these anomalies in the previous report.[3] Although one patient with a *SMOC1* mutation from family C did not show bowed tibia and hypoplastic fibula, these anomalies could be features specific to *SMOC1* mutations. Further *SMOC1* analysis of other MLA patients should delineate the phenotypic consequences caused by *SMOC1* mutations.

Accumulating evidence suggests that BMP signaling plays crucial roles in early eye vesicle and limb patterning, skeletal formation, and apoptosis of the interdigital mesenchyme,[25–29] and mutations involving BMP signaling cause human malformations including ocular, limb, and skeletal anomalies.[7,30–33] Here, we present genetic evidence that *SMOC1* is essential for ocular and limb development in humans and mice. Furthermore, *Xenopus smoc* can inhibit BMP signaling,[11] suggesting that *SMOC1/Smoc1* can also modulate BMP signaling in humans and mice. Indeed, we observed reduced and/or disturbed expression of genes involved in BMP signaling in the interdigital mesenchyme in *Smoc1* null mice, and limb and ocular abnormalities associated with loss of *Smoc1* function are consistent with phenotypic consequences of disturbed BMP signaling. Conditional inactivation of *Bmp2* in the limb showed 3/4 syndactyly, and a similar deficiency of both *Bmp2* and *Bmp7* resulted in malformed fibulae in mice.[25] Moreover, mice deficient in *Fmn1*, a repressor of BMP signaling, showed four digits, fused metatarsal bones, and an absence of fibulae in the hindlimbs,[34] suggesting the importance of altered BMP signaling in these features. Concerning ocular phenotypes, haploinsufficiency of mouse *Bmp4* resulted in a decreased number of ganglion layer cells and absence of the optic nerve similar to *Smoc1* null mice,[35] indicating that altered BMP signaling is also involved in the ocular phenotype. Interestingly, knockdown experiments of *smoc* by antisense morpholino in *Xenopus* showed absence or severe deformity of the eye and other anterior structures, which were accompanied by aberrant expression of *otx2*, *tbx2* in the eye field.[11] Mutations of *OTX2* (MIM 600037) cause micropthalmia, syndromic 5 (MCOPS5 [MIM 610125]) in humans.[36] Moreover, targeted disruption of *Tbx2* resulted in a marked reduction in the size of the optic cup and a failure of optic nerve formation in mice.[37] Thus, it is possible that loss of *SMOC1* function could alter the expression of *OTX2* and *TBX2* (MIM 600747) by disturbing BMP signaling in human developing eyes.

It is unknown how the loss of functional SMOC1, a BMP antagonist, leads to reduced expression of genes involved in BMP signaling in the interdigital mesenchyme in *Smoc1* null mice. In the case of *Fmn1*-deficient mice, the loss of the repressor of BMP signaling resulted in downregulation of *Fgf4* and *Shh* and in upregulation of *Gremlin* expression at E10.5, and absence of apoptosis of the interdigital mesenchyme between the two middle digits at E13.5.[34] Thus, there is a possibility that loss of SMOC1 could cause the imbalance among BMP, SHH, and FGF signaling, which would subsequently lead to reduced and/or disturbed expression of genes involved in BMP signaling in the interdigital mesenchyme. In fact, we observed reduced expression of *Msx2* in the progressive zone of hindlimbs at E11.5 (Figure S2). Moreover, expression of *Sox9*, the initial cartilage condensation marker, showed abnormal limb patterning, suggesting that SMOC1 may affect BMP signaling even at early stages of limb development (Figure S3). Further examinations are required for understanding spatial and temporal actions of SMOC1/Smoc1 protein during limb development.

In conclusion, our data demonstrate that *SMOC1/Smoc1* is an essential player in both ocular and limb development in humans and mice and give further support to the crucial roles of BMP signaling in these systems.

Supplemental Data

Supplemental Data include three figures and four tables and can be found with this article online at http://www.cell.com/AJHG/.

(Q) Optic nerve diameter. Optic nerves were significantly hypoplastic in *Smoc1*[Tp/Tp] mice in comparison to WT and *Smoc1*[Tp/+] littermates. The numbers of pups (B and C) or eyes (Q) corresponding to each genotype are indicated within bars. Error bars indicate standard deviation: *$p < 0.01$, compared with WT. **$p < 0.01$, compared with WT and *Smoc1*[Tp/+]. Scale bars represent 1 mm (D, E, and L–P), 200 µm (F–I), 500 µm (J and K), and 100 µm (J' and K').
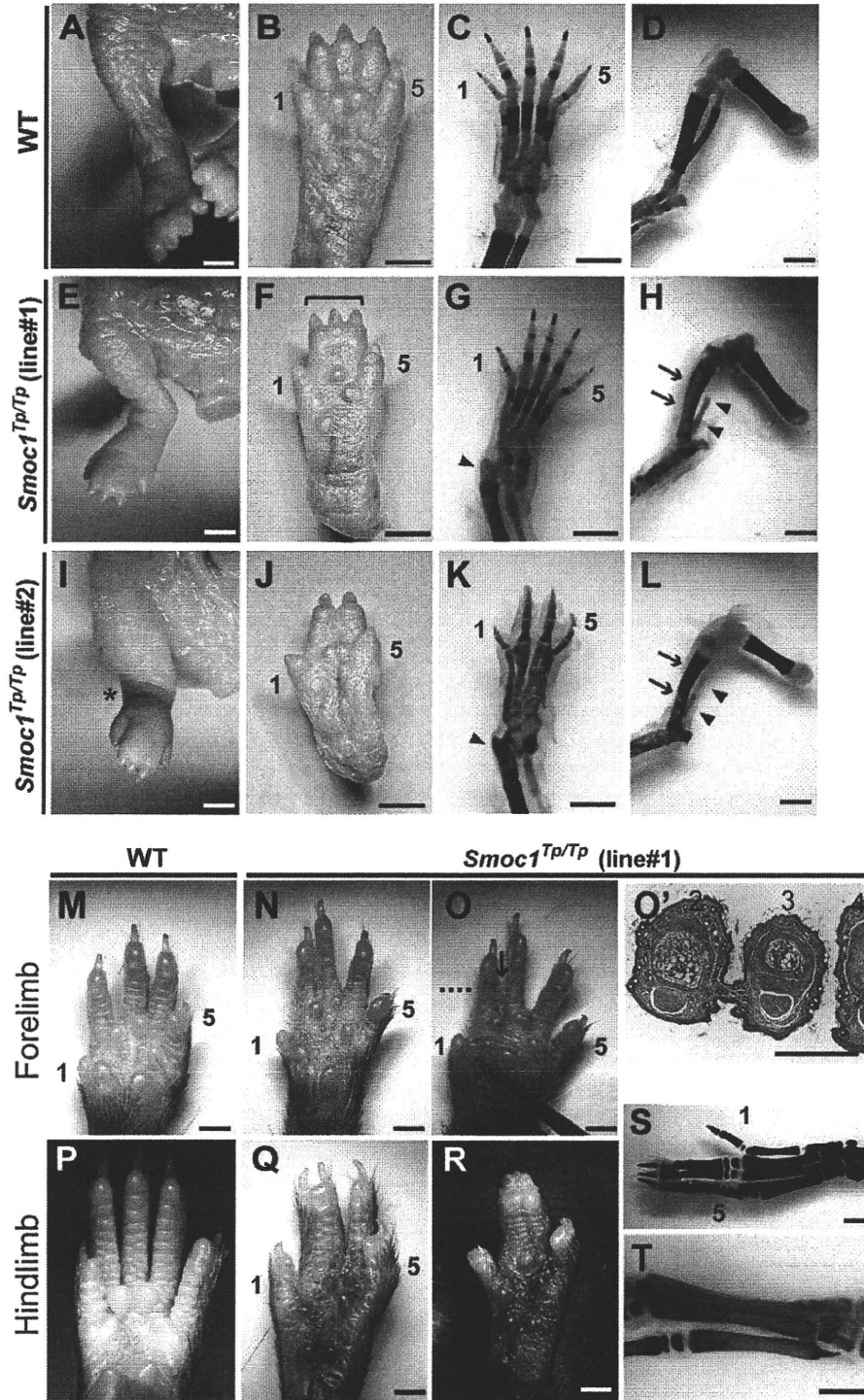
55

Figure 4. Limb Phenotypes of *Smoc1* Null Mice

Limbs of WT (A–D, M, and P) and *Smoc1*$^{Tp/Tp}$ mice (E–L, N–O', and Q–T) at P0 (A–L) and P14 (M–T). Digit identities are indicated by the numbers 1 (thumb, anterior) and 5 (little finger, posterior). Skeletal staining with alcian blue and alizarin red is presented (C, D, G, H, K, L, S, and T). *Smoc1*$^{Tp/Tp}$ mice showed pes valgus (E and I), soft tissue syndactyly (F and G), and four digits with metatarsal fusion (J and K). Malposition of the articulation between the tibia/fibula and the calcanea (G and K, magenta arrowheads), bowed tibia (magenta arrows), and hypoplastic fibula (arrowheads) of *Smoc1*$^{Tp/Tp}$ mice (H and L) were observed. 2/3 soft tissue syndactyly (N) and 2/3 webbing (O) were evident in forelimbs of *Smoc1*$^{Tp/Tp}$ mice. (O') A transverse section taken at the level indicated by the dashed line in (O) showed 2/3 webbing. 2/3 syndactyly (Q), 2/3/4 syndactyly (R), synostosis between the 2nd and 3rd proximal phalanx and metatarsals (S), and synostosis between the 4th and 5th metatarsals (T, arrow), observed in the hindlimbs of *Smoc1*$^{Tp/Tp}$ mice. Scale bars represent 1 mm (A–O and P–T) or 500 μm (O').

Table 1. Limb Abnormalities in Smoc1$^{Tp/Tp}$ Mutants

Genotype	Talipes Valgus (No. of Affected/Total No. of Pups)	Forelimb Abnormalities (No. of Limbs)	Hindlimb Syndactyly (No. of Limbs)					Other External Abnormalities (No. of Pups)	4th and 5th Metatarsal Fusion (No. of Affected/Total No. of Limbs)
			None	2/3[a]	3/4[b]	2/3/4[c]	4 Digits		
Postnatal Day 0									
Smoc1$^{Tp/+}$ (line 1, C57BL/6J)	0/42	0	84	0	0	0	0		
Smoc1$^{Tp/+}$ (line 2, ICR mixed)	0/38	0	76	0	0	0	0		
Smoc1$^{Tp/Tp}$ (line 1, C57BL/6J)	10/10	0	3	0	3	12	2		
Smoc1$^{Tp/Tp}$ (line 2, ICR mixed)	13/17	1[d]	1	1	9	4	19	cleft palate (3)	
Postnatal Day 14									
Smoc1$^{Tp/+}$ (line 1, C57BL/6J)	0/70	0	140	0	0	0	0		
Smoc1$^{Tp/Tp}$ (line 1, C57BL/6J)	11/11	18[e]	2	7	3	8	2	hypoplastic thumbs (5)	9/10[f]

[a] Syndactyly between the 2nd and 3rd digits.
[b] Syndactyly between the 3rd and 4th digits.
[c] Syndactyly between the 2nd, 3rd, and 4th digits.
[d] 2/3 soft tissue syndactyly.
[e] Eleven limbs showed 2/3 webbing, four limbs showed 2/3 soft tissue syndactyly, and one limb showed 3/4 syndactyly.
[f] Based on examination of skeletal preparations.

Web Resources

The URLs for data presented herein are as follows:

BDGP, http://www.fruitfly.org/
ESEfinder 3.0, http://rulai.cshl.edu/cgi-bin/tools/ESE3/esefinder.cgi?process=home
GenBank, http://www.ncbi.nlm.nih.gov/Genbank/
HSF2.4.1, http://www.umd.be/HSF/
NetGene2, http://www.cbs.dtu.dk/services/NetGene2/
Online Mendelian Inheritance in Man, http://www.ncbi.nlm.nih.gov/Omim

UCSC Genome Browser, http://genome.ucsc.edu/cgi-bin/hgGateway
SpliceView, http://zeus2.itb.cnr.it/~webgene/wwwspliceview.html

References

1. Waardenburg, P.J. (1961). Autosomally-recessive anophthalmia with malformations of the hands and feet. In Genetics and Ophthalmology, P.J. Waardenburg, A. Franceschetti, and D. Klein, eds. (Assen, The Netherlands: Royal Van Gorcum), p. 773.
2. Teiber, M.L., Garrido, J.A., and Barreiro, C.Z. (2007). Ophthalmo-acromelic syndrome: report of a case with vertebral anomalies. Am. J. Med. Genet. A. 143A, 2460–2462.
3. Garavelli, L., Pedori, S., Dal Zotto, R., Franchi, F., Marinelli, M., Croci, G.F., Bellato, S., Ammenti, A., Virdis, R., Banchini, G., and Superti-Furga, A. (2006). Anophthalmos with limb anomalies (Waardenburg opththalmo-acromelic syndrome): report of a new Italian case with renal anomaly and review. Genet. Couns. 17, 449–455.
4. Tekin, M., Tutar, E., Arsan, S., Atay, G., and Bodurtha, J. (2000). Ophthalmo-acromelic syndrome: report and review. Am. J. Med. Genet. 90, 150–154.
5. Adler, R., and Canto-Soler, M.V. (2007). Molecular mechanisms of optic vesicle development: complexities, ambiguities and controversies. Dev. Biol. 305, 1–13.
6. Zeller, R., López-Ríos, J., and Zuniga, A. (2009). Vertebrate limb bud development: moving towards integrative analysis of organogenesis. Nat. Rev. Genet. 10, 845–858.
7. Bakrania, P., Efthymiou, M., Klein, J.C., Salt, A., Bunyan, D.J., Wyatt, A., Ponting, C.P., Martin, A., Williams, S., Lindley, V., et al. (2008). Mutations in BMP4 cause eye, brain, and digit
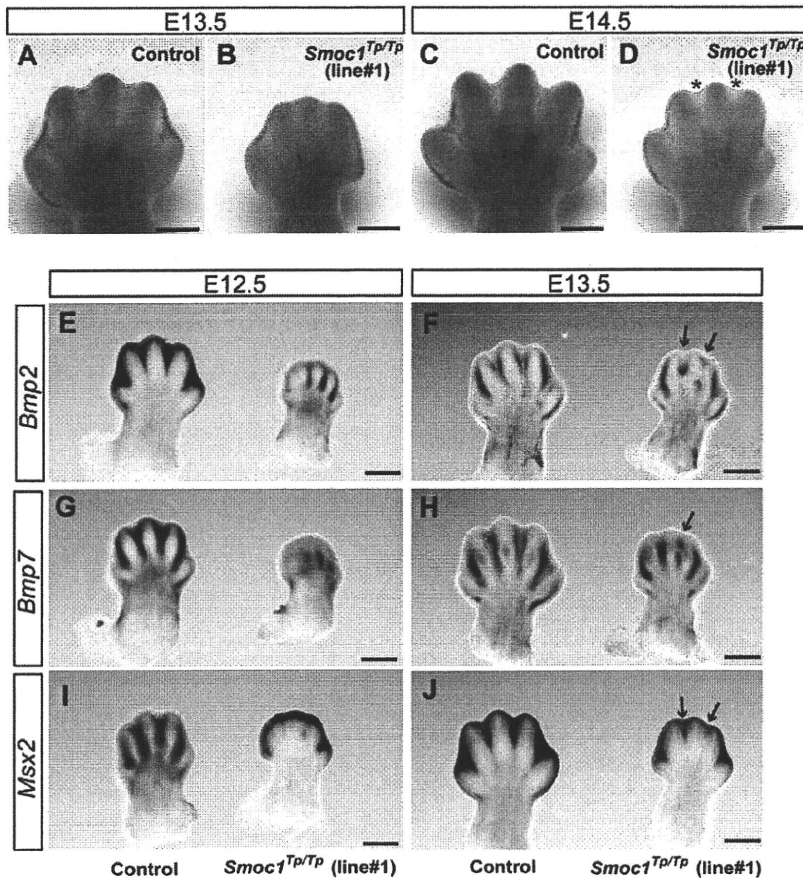
57

Figure 5. Reduced Apoptosis and Altered BMP Signaling in the Interdigital Mesenchyme of *Smoc1* Null Mice

(A–D) NB staining of left hindlimbs at E13.5 (A and B) and E14.5 (C and D). In comparison to control embryos (WT and $Smoc1^{Tp/+}$ littermates) (A and C), the number of NB-stained apoptotic cells in the interdigital mesenchyme of $Smoc1^{Tp/Tp}$ mice was dramatically reduced between digits 2 and 3 and digits 3 and 4 at both E13.5 and E14.5, and the webbing remained at a distal level (B and D, magenta asterisk).

(E–J) Whole-mount in situ hybridization of right hindlimbs at E12.5 (E, G, and I) and E13.5 (F, H, and J). At E12.5, interdigital expression of *Bmp2*, *Bmp7*, and *Msx2* was profoundly delayed in the hindlimbs of $Smoc1^{Tp/Tp}$ mice, and their expression in the interdigital mesenchyme was apparently perturbed, even at E13.5 (magenta arrows). Scale bar represents 500 µm.

developmental anomalies: overlap between the BMP4 and hedgehog signaling pathways. Am. J. Hum. Genet. *82*, 304–319.

8. Bornstein, P., and Sage, E.H. (2002). Matricellular proteins: extracellular modulators of cell function. Curr. Opin. Cell Biol. *14*, 608–616.

9. Vannahme, C., Smyth, N., Miosge, N., Gösling, S., Frie, C., Paulsson, M., Maurer, P., and Hartmann, U. (2002). Characterization of SMOC-1, a novel modular calcium-binding protein in basement membranes. J. Biol. Chem. *277*, 37977–37986.

10. Gersdorff, N., Müller, M., Schall, A., and Miosge, N. (2006). Secreted modular calcium-binding protein-1 localization during mouse embryogenesis. Histochem. Cell Biol. *126*, 705–712.

11. Thomas, J.T., Canelos, P., Luyten, F.P., and Moos, M., Jr. (2009). Xenopus SMOC-1 inhibits BMP signaling downstream of receptor binding and is essential for post-gastrulation development in Xenopus. J. Biol. Chem. *284*, 18994–19005.

12. Hamanoue, H., Megarbane, A., Tohma, T., Nishimura, A., Mizuguchi, T., Saitsu, H., Sakai, H., Miura, S., Toda, T., Miyake, N., et al. (2009). A locus for ophthalmo-acromelic syndrome mapped to 10p11.23. Am. J. Med. Genet. A. *149A*, 336–342.

13. Mégarbané, A., Souraty, N., and Tamraz, J. (1998). Ophthalmo-acromelic syndrome (Waardenburg) with split hand and polydactyly. Genet. Couns. *9*, 195–199.

14. Cogulu, O., Ozkinay, F., Gündüz, C., Sapmaz, G., and Ozkinay, C. (2000). Waardenburg anophthalmia syndrome: report and review. Am. J. Med. Genet. *90*, 173–174.

15. Miyake, N., Kosho, T., Mizumoto, S., Furuichi, T., Hatamochi, A., Nagashima, Y., Arai, E., Takahashi, K., Kawamura, R., Wakui, K., et al. (2010). Loss-of-function mutations of CHST14 in a new type of Ehlers-Danlos syndrome. Hum. Mutat. *31*, 966–974.

16. Gudbjartsson, D.F., Thorvaldsson, T., Kong, A., Gunnarsson, G., and Ingolfsdottir, A. (2005). Allegro version 2. Nat. Genet. *37*, 1015–1016.

17. Keng, V.W., Yae, K., Hayakawa, T., Mizuno, S., Uno, Y., Yusa, K., Kokubu, C., Kinoshita, T., Akagi, K., Jenkins, N.A., et al. (2005). Region-specific saturation germline mutagenesis in mice using the Sleeping Beauty transposon system. Nat. Methods *2*, 763–769.

18. Mamo, S., Gal, A.B., Bodo, S., and Dinnyes, A. (2007). Quantitative evaluation and selection of reference genes in mouse oocytes and embryos cultured in vivo and in vitro. BMC Dev. Biol. *7*, 14.

19. Parr, B.A., Shea, M.J., Vassileva, G., and McMahon, A.P. (1993). Mouse Wnt genes exhibit discrete domains of expression in the early embryonic CNS and limb buds. Development *119*, 247–261.

20. Saitsu, H., Ishibashi, M., Nakano, H., and Shiota, K. (2003). Spatial and temporal expression of folate-binding protein 1 (Fbp1) is closely associated with anterior neural tube closure in mice. Dev. Dyn. *226*, 112–117.

21. Tamplin, O.J., Kinzel, D., Cox, B.J., Bell, C.E., Rossant, J., and Lickert, H. (2008). Microarray analysis of Foxa2 mutant mouse embryos reveals novel gene expression and inductive roles